SCIENCE CHINA Materials

REVIEWS

mater.scichina.com link.springer.com

Published online 13 August 2019 | https://doi.org/10.1007/s40843-019-9468-5

Sci China Mater 2019, 62(11): 1679–1708

SPECIAL ISSUE: Celebrating the 100th Anniversary of Nankai University

Copper nanomaterials and assemblies for soft electronics

Yang Feng[1,2] and Jian Zhu[1,2,3,4*]

ABSTRACT **Soft electronics that can simultaneously offer electronic functions and the capability to be deformed into arbitrary shapes are becoming increasingly important for wearable and bio-implanted applications. The past decade has witnessed tremendous progress in this field with a myriad of achievements in the preparation of soft electronic conductors, semiconductors, and dielectrics. Among these materials, copper-based soft electronic materials have attracted considerable attention for their use in flexible or stretchable electrodes or interconnecting circuits due to their low cost and abundance with excellent optical, electrical and mechanical properties. In this review, we summarize the recent progress on these materials with the detailed discussions of the synthesis of copper nanomaterials, approaches for their assemblies, strategies to resist the ambient corrosion, and their applications in various fields including flexible electrodes, sensors, and other soft devices. We conclude our discussions with perspectives on the remaining challenges to make copper soft conductors available for more widespread applications.**

Keywords: copper nanomaterials, assemblies, composites, stretchable conductors, soft electronics

INTRODUCTION

The elastic, soft, and nonplanar electronics inspired by biological systems overcome the fundamental limits imposed by the rigid silicon-based electronics, and expand the horizon of electronics applications unforeseeable in the past [1–3]. These soft electronics enable the more approachable network of internet of things, and allow the future electronics to take more crucial roles in health monitoring, soft robotics, electronic skins and biological sensors [4–7]. Flexible and highly conductive conductors are playing a vital role in these advanced electronics, including wearable electronics [5,8–12], stretchable transistors [13], ultrasensitive and selective non-enzymatic glucose detection [14], flexible solar cells [15], stretchable organic light-emitting diodes (LEDs) [16,17], biosensors or biomimetic sensors [6,18], actuators [19,20], energy harvesting devices [21–28] and so on. One way to realize these soft conductors needs intimate and robust integration of highly conductive metal nanomaterials with mechanically stretchable elastomers. The optimized soft conductors have the ability to be twisted or bent, and easily conform to curvilinear surfaces, or maintain highly conductive characteristics under large strains (>>1%) and recover their initial performance with released stress [29]. The nanomaterials made of noble metals, such as gold or silver, have attracted intense attention as the conductive components in deformable electronics due to their high conductivity and inertness against oxidation [5,6,18,30,31]. However, the use of noble metals in flexible electronics is intrinsically limited by their high cost due to their scarcity on earth. As an alternative to these noble metals, much less expensive copper is receiving increasing interest, and it may act as a potential contender to completely replace noble metals in soft electronic circuits. As a comparison, copper has an electrical resistivity of 1.75×10^{-8} Ω m, comparable to that of silver (1.65×10^{-8} Ω m) and gold (2.40×10^{-8} Ω m), yet is 1000 times more abundant and 100 times less expensive than silver [32]. Despite these advantages, copper suffers from easy oxidation in the ambience, and may lose its conductivity easily. In addition, the morphologies and surface chemistry of copper nanomaterials should be further optimized to enable the proper interface for the integration with elastomers. The ultimate

[1] School of Materials Science and Engineering, Nankai University, Tianjin 300350, China
[2] National Institute for Advanced Materials, Nankai University, Tianjin 300350, China
[3] Tianjin Key Laboratory of Metal and Molecule-Based Material Chemistry, Nankai University, Tianjin 300350, China
[4] Tianjin Key Laboratory for Rare Earth Materials and Applications, Nankai University, Tianjin 300350, China
* Corresponding author (email: zj@nankai.edu.cn (Zhu J))

goal is to achieve copper-based soft conductors with a balance of high conductivity and stretchability, as well as high stability in the atmosphere. To this end, a lot of efforts have been devoted to the synthesis of the copper nanomaterials and their implementation in elastomeric conductors [33–35].

Excited by the advancements in the soft electronics enabled by the copper-based conductors, we intend to summarize the recent progress in this emerging field in the review. The following discussion is divided into six parts. The first part discloses our survey on the recent synthesis methods of zero-, one- and two-dimensional (0D, 1D, and 2D) copper nanomaterials, i.e., copper nanoparticles (CuNPs), copper nanowires (CuNWs), and copper nanoflakes (CuNFs). The second part reveals a variety of techniques to assemble copper nanomaterials into macroscopic soft conductors, including spray coating, spin coating, vacuum assisted assembly and transfer, doctor-blade coating, screen printing, and controlled ink patterning. The third part examines the intrinsic electrical and mechanical properties of copper nanomaterials. The fourth part details various strategies to make copper-based conductors less sensitive to degradation. The fifth part further delves into various electronic applications of copper-based soft conductors, exemplified by stretchable conductors, flexible transparent electrode, solar cells, LEDs, electromechanical sensors and wearable heaters. In the last part, we provide our outlook into the potential future directions to address the remaining challenges in the field of copper-based soft conductors and electronics.

SYNTHESIS OF COPPER NANOMATERIALS

Copper-based soft conductors are usually prepared by manipulating a proper combination between copper nanomaterials and elastomeric or flexible polymers. The network of copper nanomaterials forms conductive pathways to allow the electrons to hop or tunnel through, while the polymers provide a flexible support to tolerate the mechanical deformation of the conductive networks. In these copper nanomaterials/polymer composites, the quality, surface chemistry, and morphologies of copper nanomaterials play crucial roles in affecting the electric conductivity of soft conductors and their behaviors under deformation. In this part, we inspect the synthesis methods for the library of copper nanomaterials, encompassing CuNPs (0D), CuNWs (1D), CuNFs (2D).

Copper nanoparticles

CuNPs, sometimes also refereed as 0D copper nanocrystals, are the typical copper nanomaterials used for soft conductors. The 0D characteristics with sizes typically below 100 nm make CuNPs easily formulate into conductive inks or pastes for printing various electronic components.

Similar to the synthesis of other nanocrystals, the synthetic recipe of CuNPs usually involves a copper precursor, a reducing agent, and sometimes a surfactant, the combination of which finely tunes the sizes, dispersibility and uniformity of CuNPs [36–45]. The formation of CuNPs involves nucleation and growth stages, generally following the famous LaMer mechanism [46]. This mechanism is generally described as a process involving three successive phases (Fig. 1a): (1) the rapid increase of monomers through the decomposition of precursors when the temperature is raised; (2) the burst nucleation at a supersaturated concentration of monomers; (3) the continued growth of nuclei into mature nanocrystals with the supply of monomers diffused from solution [46–48]. The prolonged growth may trigger the classical Ostwald ripening stage leading to a broadened distribution of nanocrystal products [47]. Successful utilization of CuNPs relies on the synthesis methods that are capable of controlling the size distribution of CuNPs and easy to scale up. There has been a myriad of interesting studies conducted to fulfill this pragmatic goal.

CuNPs have been synthesized in aqueous solutions with high yields using $CuSO_4$ as the precursor, ascorbic acid as the reductant, and cetyltrimethylammonium bromide (CTAB) as the cationic surfactant and also the capping agent [36]. The produced CuNPs were confirmed by energy-dispersive X-ray spectroscopy (EDS) and X-ray diffraction (XRD) to be pure copper with face-centered cubic (fcc) structures and an average diameter of 90 nm. In order to better control the sizes of CuNPs and make the synthesis more readily scalable, a modified reverse micelle method was used by reacting copper(II) acetate and *L*-ascorbic acid in a solution containing water and xylene in the presence of oleic acid and oleylamine as the surfactants. The synthesized CuNPs had a nearly spherical profile and multiple-twinned structures, and sizes ranging between 15 and 100 nm with narrow distributions [45]. In addition to the reverse micelle method, the polyol method has been used to control the sizes of monodispersed CuNPs. The reactions took place in diethyleneglycol with $CuSO_4$ as the precursor, and sodium phosphinate as the reducing agent, and poly(*N*-vinylpyrrolidone) (PVP) as the capping molecule at the reaction temperature of 140°C. Scanning electron microscopy (SEM) shows CuNPs have a spherical mor-

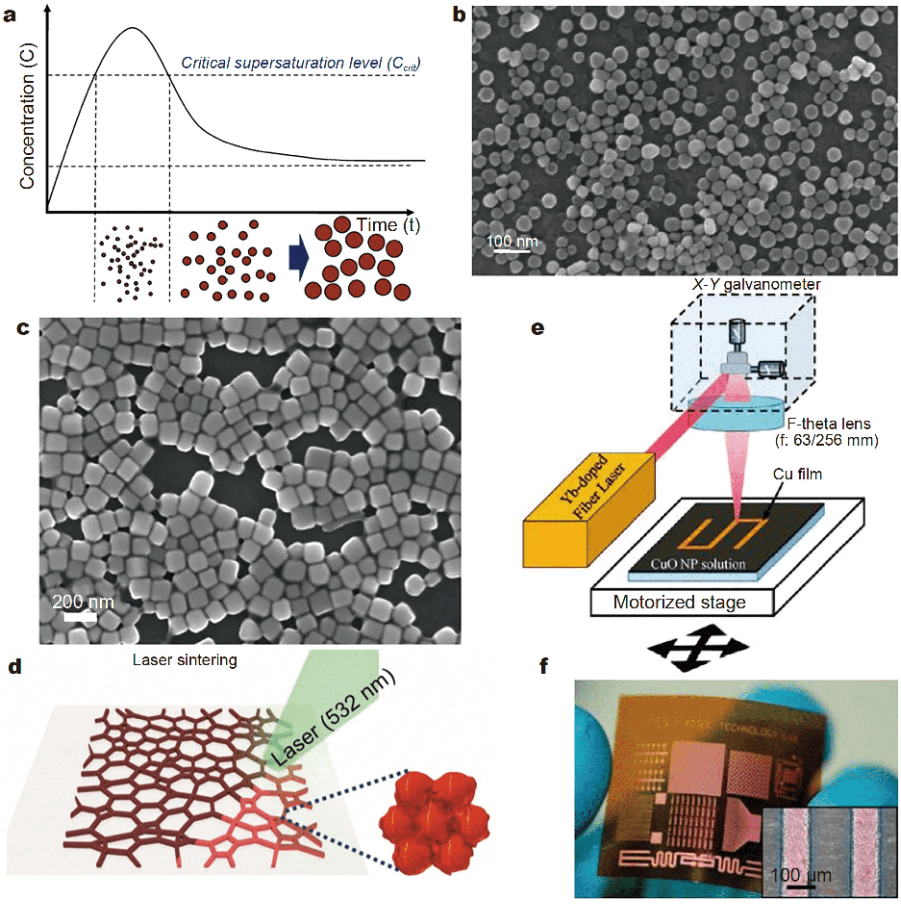

Figure 1 Synthesis of CuNPs. (a) Schematic illustration of nucleation and growth mechanisms based on LaMer's model for the monodispersed particles. (b) SEM image of the synthesized CuNPs at the reaction temperature of 140°C with the homogenous size distribution. (a, b) Reprinted with permission from Ref. [40]. Copyright 2007, Elsevier. (c) SEM images of Cu nanocubes. The edge lengths of the nanocubes is about 100 nm. Reprinted with permission from Ref. [37]. Copyright 2011, Wiley-VCH. (d) Schematic for Cu conductive electrode fabricated by CuNPs inks and a crack template. The CuNPs network transferred to a PET substrate film was sintered by 532 nm visible laser to obtain close-packed structure of the NPs by melting. Reprinted with permission from Ref. [44]. Copyright 2016, Wiley-VCH. (e) Schematic of the experimental setup. The CuO NPs are transformed into Cu film by photochemical reduction and photothermal agglomeration, and (f) optical photo and microscopic image (inset) of copper electrodes on a PI film. Reprinted with permission from Ref. [38]. Copyright 2011, American Chemical Society.

phology with a diameter range of 45±8 nm (Fig. 1b) [40]. This polyol method did not require special inert environments to protect CuNPs against oxidation, and the CuNPs maintained intact in air due to the use of non-aqueous solvent as the reaction medium and capping agent PVP, effectively preventing the oxidation process [40]. Aside from spherical CuNPs, cubic CuNPs were synthesized with $CuCl_2$ as the precursor, glucose as the reductant, and hexadecylamine (HDA) as the capping agent (Fig. 1c). HDA concentration played an important role in dictating the morphology from CuNWs to CuNPs, while the edge lengths of cubic CuNPs were tuned from 50 to 200 nm with the increase of reaction time [37].

The synthesized CuNPs are typically covered with a layer of capping agents, which greatly facilitates their dispersion in selected solvents, and the topmost Cu atoms tend to be oxidized under the exposure of air forming CuO. These insulating barriers impede the electron transfer between different CuNPs, thus rendering a poor conductivity of their macroscopic assemblies. While CuNPs inks can be easily prepared and casted into thin films (more discussions in Section of "Approaches for the assembly of copper nanomaterials for soft conductors"), thermal [49] or optical activation [38,44] is needed to convert the oxide layer into conductive Cu. The thermal or optical energy makes the assemblies of CuNPs more compact. 532 nm laser was found to be effective in sintering CuNPs networks templated by cracks into a more conductive close-packed structure (Fig. 1d). The selective reduction of CuO into Cu by laser makes possible the

patterning of Cu directly from CuO NPs. It was found that the Cu patterns were easily attained by irradiating films of CuO NPs on a digitally programmed motorized stages by 1070 nm laser (Fig. 1e) [38]. The Cu electrodes formed in this way had a decent resistivity of 31 μΩ cm and could be deposited on a polyimide (PI) film (Fig. 1f) [38].

Copper nanowires

One-dimensional CuNWs are important copper nanomaterials that are attracting tremendous interest. The high aspect ratio of CuNWs makes it easy to form a percolation network at a relatively low concentration in the assembled structure. In addition, the ultrathin nature of CuNWs enables the intrinsic flexibility of CuNWs, and the porous networks consisting of CuNWs make the stretchability possible due to the sliding movement along the length direction under the stress. Therefore, there are a multitude of studies devoting to synthesizing CuNWs with long lengths, uniform distributions, high yields in a simple and scalable process. Among the wide variety of methods available to synthesize CuNWs, solution-based synthesis routes are considered to be a promising strategy because of several advantages including wide selection of precursors, solvents and reaction conditions, and the feasibility of low-cost production [37].

Similar to the synthesis of CuNPs, the morphological control of CuNWs is dependent on the choice of copper precursors, reducing agents, and the capping agents or surfactants under suitable reaction conditions. Hydrothermal methods with reactions occurring in an autoclave under a high pressure and a high temperature are one of the facile ways for the production of CuNWs in large scale. Depending on the reaction conditions, the synthesized CuNWs may have the single crystal structure of fcc Cu along the $[1\bar{1}0]$ growth direction, or the five-fold twinned pentagonal structure growth along the [110] direction. A surfactant-assisted hydrothermal reduction approach was proposed for the synthesis of CuNWs with average diameters of ~85 nm and lengths of ~10 μm [50]. In their synthesis, the Cu(II)-glycerol complexes (Cu($C_3H_6O_3$)) were reduced by phosphite (HPO_3^{2-}) at 120°C with sodium dodecyl benzenesulfonate (SDBS) as the surfactant [50]. The single crystalline CuNWs originated from the seeded growth from the fcc Cu nanocrystals obtained in the initial stage, and had a preferred $[1\bar{1}0]$ growth direction, while SDBS was served as a guiding agent for kinetically controlling the growth rates of various crystallographic facets [50]. Another surfactant-assisted reduction approach was proposed later with the reducing and capping agents of hydrazine and ethylenediamine (EDA) respectively for the synthesis of CuNWs from $CuNO_3$ in the very basic (NaOH) conditions (Fig. 2a) [51]. The high concentration of NaOH was necessary to prevent copper ions forming $Cu(OH)_2$ precipitates. Both NaOH and EDA were important for regulating the proper growth of the 1D product. CuNWs had a diameter of 90–120 nm, and a length of 40–50 μm, corresponding to an aspect ratio of 350–450. This approach was further modified and scaled up by 200 times for 1.2 g product of CuNWs [52], showing its potential for large-scale production (Fig. 2b). The CuNWs were 90 ±10 nm in diameter and 10±3 μm in length. The growth mechanism of CuNWs was reconfirmed as a scenario in which CuNWs grew from the seeding spherical NP. The same research group revealed more insight into the growth mechanism recently using a facet selective electrochemistry [53]. EDA increased the reduction rate for copper on a Cu(111) surface in comparison to Cu(100) by selectively inhibiting the formation of copper oxide on Cu (111), thereby leading to the 1D growth of Cu (Fig. 2c). Rather than the prevailing hypothesis that a capping agent generally blocks the addition of atoms to specific crystal facets. EDA actually increases the reduction rate of Cu atoms to Cu(111) facets in the NaOH-EDA-Cu $(NO_3)_2$-N_2H_4 system.

Other than EDA, other alkylamines, such as octadecylamine (ODA) or HDA, have been used as capping agents or even reducing agents for the synthesis of CuNWs in aqueous media [37,58–62]. It was found that ODA could directly convert copper(II) ions into ultralong and uniform CuNWs with uniform and controllable diameters of 30–100 nm, length up to several millimeters (aspect ratio $>10^5$) by the hydrothermal processing of the complex emulsion of $CuCl_2$ and ODA at 120–180°C without the assistance of other reducing agents or surfactants. The obtained CuNWs were polycrystalline when the reaction occurred at 120°C, and were single crystalline at 180°C [58]. The use of a shorter alkylamine, HDA and glucose as the additional reducing agent, reduced the required temperature for single crystalline CuNWs to 120°C [61]. With an optimum ratio between HDA and glucose, the obtained CuNWs had a uniform diameter of 64±8 nm, and a length of a few micrometers (aspect ratio >50). This method was further optimized to yield a diameter of 24±4 nm, and a length of tens to hundreds of micrometers or even several millimeters at an even lower temperature of 100°C (Fig. 2d). Based on the SEM and high-resolution transmission electron microscope (HRTEM) results, the obtained CuNWs were confirmed to have a penta-twin-

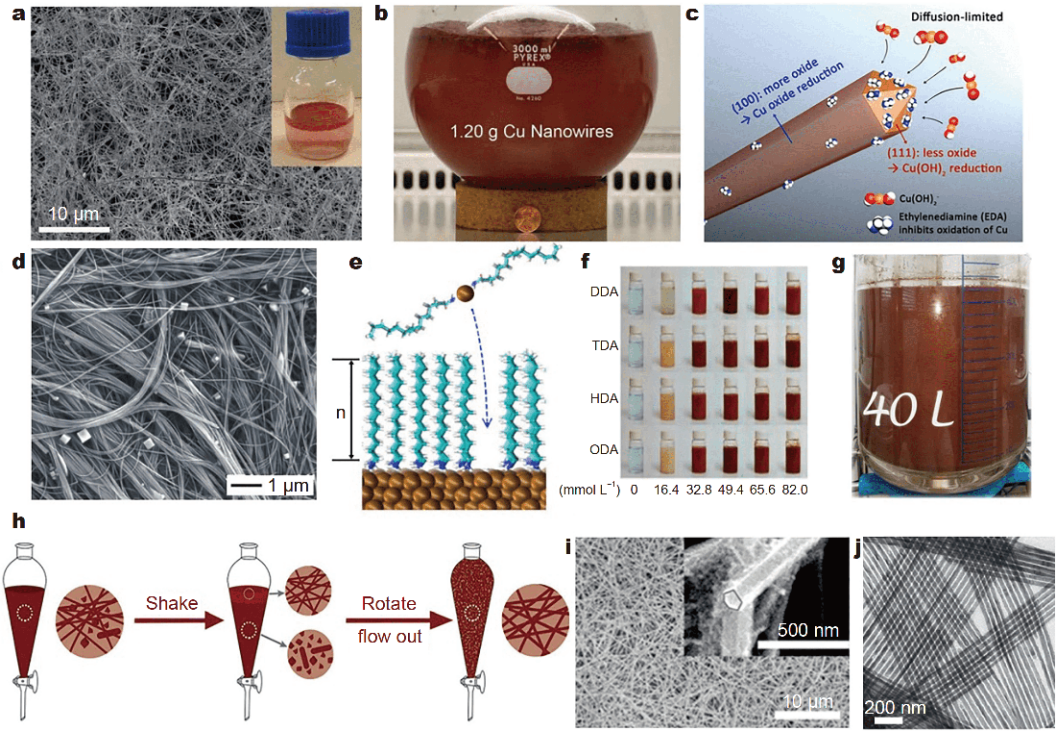

Figure 2 Synthesis of CuNWs by wet chemistry. (a) SEM image of CuNWs, the inset is the as-prepared CuNWs in the mother liquid. Reprinted with permission from Ref. [51]. Copyright 2005, American Chemical Society. (b) Picture of the reaction flask after the growth of CuNWs at 80°C for 1 h. Reprinted with permission from Ref. [52]. Copyright 2010, Wiley-VCH. (c) Schematic diagram of CuNWs growth in the NaOH-EDA-$Cu(NO_3)_2$-N_2H_4 system. Reprinted with permission from Ref. [53]. Copyright 2017, American Chemical Society. (d) SEM image of the CuNWs prepared using the standard procedure. Reprinted with permission from Ref. [37]. Copyright 2011, Wiley-VCH. (e) Image for the absorption of long-chain alkylamine (*n*=carbon number) to their monolayers on the Cu (111) surface. (f) Images showing the color of the reaction solutions containing different types and concentrations of alkylamines (dodecylamine (DDA), tetradecylamine (TDA)) after heating at 90°C for 16 h. Reprinted with permission from Ref. [54]. Copyright 2018, American Chemical Society. (g) Photograph of the 40 L concentrated large-scale synthesis in a borosilicate glass reaction vessel. (h) Scheme of the shaking-rotating technique process to separate CuNWs from the byproducts successfully. Reprinted with permission from Ref. [55]. Copyright 2019, American Chemical Society. (i) SEM image of formed CuNWs directed by the liquid-crystalline structure of the medium. Reprinted with permission from Ref. [56]. Copyright 2012, American Chemical Society. (j) High-magnification TEM of the ultralong CuNWs synthesized in an oleylamine solution. Reprinted with permission from Ref. [57]. Copyright 2013, the Royal Society of Chemistry.

ned structure bound by ten {111} facets at the two ends and five {100} facets at the side. The increase of glucose concentration from 5 to 10 mg mL^{-1} led to the growth of tadpole-like CuNWs originating from the tapered Cu nanocrystals formed during the seeding stage. The growth mechanism for the hydrothermal reaction of Cu^{2+} and glucose with the presence of HDA was further studied recently [54]. The more stable self-assembled monolayer of longer-chain alkylamines on the Cu (111) surface (Fig. 2e) led to greater inhibition of surface oxidation and directed the orientation of growth. The colors of the reaction solutions containing different lengths and concentrations of alkylamines are compared in Fig. 2f after the reaction [54]. It was found that glucose alone could not reduce Cu ions to metallic Cu, and rather a Maillard reaction took place between alkylamines and glucose and that this reaction was necessary to produce the reductones which in turn reduced Cu ion complexes [54,63]. This reaction was further optimized for the scale up using an *in-situ* seed-mediated two-step strategy to synthesize well-defined CuNWs in high yield, which was 2.4 times higher than that of the conventional methods with the assistance of Cu nanodots formed in the seeding step. Fig. 2g shows the photograph of the 40 L concentrated large-scale synthesis in a borosilicate glass reaction vessel. The CuNWs were easily separated from the CuNPs byproduct through an effective shaking-rotating purification technique (Fig. 2h). 50 g of high-quality CuNWs was produced with a uniform size and high aspect ratio at a very low material cost of \$ 0.99 g^{-1}, which not only provided a high-yield and low-cost synthetic route but also promoted the potential commercialization

of CuNWs in advanced nanodevices [55].

CuNWs can be synthesized directly in alkylamines, which play the role of the solvent, the capping agent, and sometimes the reducing agent. Thanks to the liquid-crystalline structure of molten HDA and CTAB mixtures at elevated temperatures of 180°C, single crystalline CuNWs with hexagonal cross sections have been synthesized at the presence of catalytic Pt surface, and they exhibited an average diameter of 78 nm, and a length up to several millimeters (Fig. 2i). The single crystalline CuNWs are expected to be more conductive and more difficult to oxidize in comparison to the penta-twinned crystalline CuNWs [56]. Oleylamine has also been used as a reaction media for the synthesis of CuNWs. High-quality CuNWs with an average diameter of approximately 50 nm and length over 10 μm at a reaction temperature of 200°C were produced from CuCl through the controlled disproportionation of Cu^+ in oleylamine. A subsequent ligand exchange of oleylamine with trioctylphosphine led to the self-assembly of CuNWs into straight bundles [60]. What is more, the addition of nickel ions was effective in catalyzing the growth of CuNWs in oleylamine. Ni(II) ions were capable of being reduced by oleylamine to Ni(0), which was further oxidized back to Ni(II) ions during the galvanic replacement reaction with Cu(II) ions, thus serving the role of catalysts. The CuNWs synthesized at a reaction temperature of 170°C have a much small diameter of 16.2±2 nm, and a length up to 40 μm with a five-fold twinned pentagonal structure [64]. Other additives, such as $RuCl_3$, were found to regulate the growth of five-fold twinned CuNWs (Fig. 2j), which had an average diameter of 22 nm, and a length of 20 μm at a reaction temperature of 170°C. Further increasing the reaction temperature and time led to the growth of bimetallic CuRu nanotubes [57]. The addition of other reducing agents, such as tris(trimethylsilyl)silane, facilitated the growth of CuNWs in oleylamine from $CuCl_2$ at a reaction temperature of 165°C, yielding an average diameter of 17.5 nm and a mean length of 17 μm [65].

CuNWs are also effectively produced by electrospinning, which makes use of electrostatic stretching of polymer fluids, such as a polymer solution or melt, through a "Taylor cone" into nanoscale polymeric filaments [66–70]. The polymer fluids for electrospinning CuNWs are a mixture of copper salts and polymer, such as copper acetate or $CuSO_4$ and poly(vinyl acetate) or PVP [70–73]. The obtained nanofibers further went through oxidation to form CuO nanofibers and were subject to reduction in H_2 environment for the production of CuNWs (Fig. 3a). The average diameters of CuNWs were controlled within the range of 50–200 nm by adjusting electrospinning conditions such as the polymer solution viscosity and the spinning voltage, and the length was over 1 cm with a diameter of ~100 nm, resulting in extremely high aspect ratios above 10^5 [73]. In addition, CuNWs have been uniaxially aligned using parallel electrodes as a collector (Fig. 3b), and this approach has improved the performance of the transparent conductor comprising Cu nanofiber networks on polydimethylsiloxane (PDMS) [73]. What's more, CuNWs were obtained by mixing CuNPs with polyacrylonitrile (PAN) and then electrospinning into nanofibers in one step [74,75]. The diameter of the Cu-PAN nanofibers ranged from 386 to 922 nm by adjusting the content of CuNPs in the polymer solution [74].

Another way to produce CuNWs using electrospinning directly exploits the electrospun polymeric nanofibers as the templates with subsequent deposition of Cu on the fiber surface [66,67,76]. For example, CuNWs were fabricated by electroless depositing Cu on the electrospun PVP NW networks, with diameters ranging from 140 to 500 nm [66]. Other than electroless deposition, Cu can be electroplated on the polymeric surface facilitated by the seeding layer of platinum or gold sputtered before the deposition (Fig. 3c) [67]. CuNWs, fabricated by electroplating of Cu onto the seeded polymers, tended to bond together in the process (Fig. 3d), thus dramatically reducing the contact resistances at the junctions [67]. The electrospun nanofibers have been used as a mask template for etching a Cu thin film into a network of CuNWs [76]. In one instance [76], poly(vinyl butyral) (PVB) fibers electrospun on Cu films were used as the etching masks, which were solvent-annealed to improve the adhesion to the Cu substrate in order to suppress the negative effect of an undercut. CuNWs were obtained using an etchant of HCl and $FeCl_3$, and PVB masks were subsequently removed by soaking in acetone during sonication [76].

Copper nanoflakes

2D CuNFs may be a potential copper nanomaterial for assembling effective soft conductors due to the high aspect ratios of the 2D geometries and large contact areas between each NF which may reduce the contact resistance. The sizes of CuNFs are easily tuned from tens of nanometers to several micrometers, making CuNFs suitable for being incorporated into conductive inks for patterning different types of electronic components. Similar to the synthesis of CuNPs and CuNWs, the synthetic recipe of CuNFs typically involves a copper precursor, a reducing agent, and some specific surfactant,

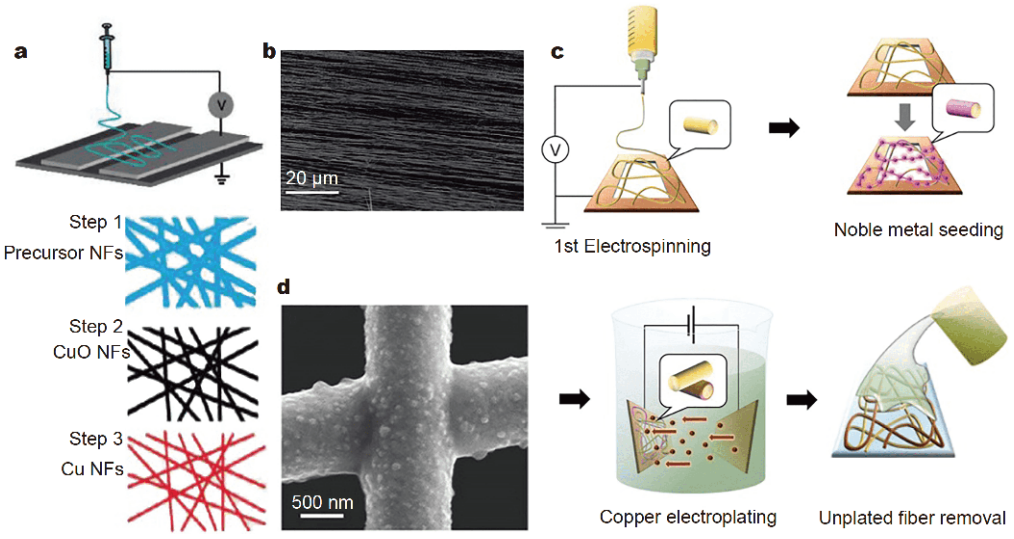

Figure 3 Fabrication of CuNWs by electrospinning. (a) Schematic of an electrospinning setup. (b) SEM image of CuNWs with uniaxially aligned arrays. (a, b) Reprinted with permission from Ref. [73]. Copyright 2010, American Chemical Society. (c) The preparation process of the CuNWs. The electrospun polymer nanofibers are deposited onto a copper frame, which are made conductive by metal seeding using an electroless non-vacuum chemical bath deposition of platinum. Copper fibers are fabricated by electroplating on to the seeded polymers, and the nonelectroplated nanofibers are removed by chemical dissolution. (d) SEM image of CuNWs fabricated by electrospinning. Reprinted with permission from Ref. [67]. Copyright 2016, Wiley-VCH.

the combination of which can finely tune the edge length, shape, dispersibility and uniformity of CuNFs under suitable reaction conditions [77].

Single-crystalline CuNFs have been synthesized from copper acetate at a temperature as low as 60°C within just 3–4 min [78]. Hydrazine was used as the reducing agent, and PVP as the surfactant and stabilizer without the need for inert atmosphere. The shapes of the single-crystalline CuNFs showed a planar morphology with a truncated triangular base and mostly into hexagons (Fig. 4a). The mean equivalent diameter counted from more than one hundred flakes was around 48.2±7.8 nm, and the average thickness of the CuNFs was determined to be 19.5± 1.5 nm by measuring the platelets perpendicular to the TEM grid (Fig. 4b) [78].

The shape and size of the CuNFs are controlled by the type and concentration of the reductants and surfactants, as well as the pH values of the solution-phase process. Larger hexagonal CuNFs with equivalent diameters of 800–1200 nm were obtained (Fig. 4c) by reducing Cu^{+} (CuCl as the copper precursor) with ascorbic acid in the presence of a surfactant of CTAB under a hydrothermal condition of 120°C for 1 h. CTAB played an important role in the formation of the CuNFs. When CTAB was substituted by cetyltrimethylammonium chloride, the obtained product changed to CuNWs [77].

More efforts have been expended into the search for larger-size CuNFs. Thin triangular CuNFs with the edge length up to several micrometers (Fig. 4d) have been synthesized with CTAB as the capping reagent and ascorbic acid as the reductant at the optimal condition of CTAB concentration of 0.06 mol L^{-1}, pH 7, and a temperature of 85°C for 2.5 h [79]. The morphology of CuNFs was tuned markedly by the CTAB concentration and pH value. The growth mechanism of these CuNFs is depicted in Fig. 4e. In the initial stage, Cu^{2+} ions are reduced by ascorbic acid, and CTAB selectively adsorbs onto the special facets of the freshly formed CuNPs, preventing the further growth of the adsorbed surface before the formation of triangular sub-CuNFs. Meanwhile, CTAB forms micro triangular micelles and acts as soft templates, in which the triangular sub-CuNFs regularly assemble themselves along the edge of the template into a triangular frame. Gradually, free triangular sub-CuNFs fill up the interior of the frame, finally forming uniform CuNFs with well-defined planar structures of thin triangular sheets [79].

In summary, the final shapes of Cu nanomaterials are determined during the nucleation and growth stages. Controlled by the initial reduction rate, the Cu seeds can be homogenous single crystalline seeds, irregularly shaped polycrystalline seeds, or individually dispersed pentagonally twinned decahedral seeds. During the growth stage, the capping agents play a crucial role in the

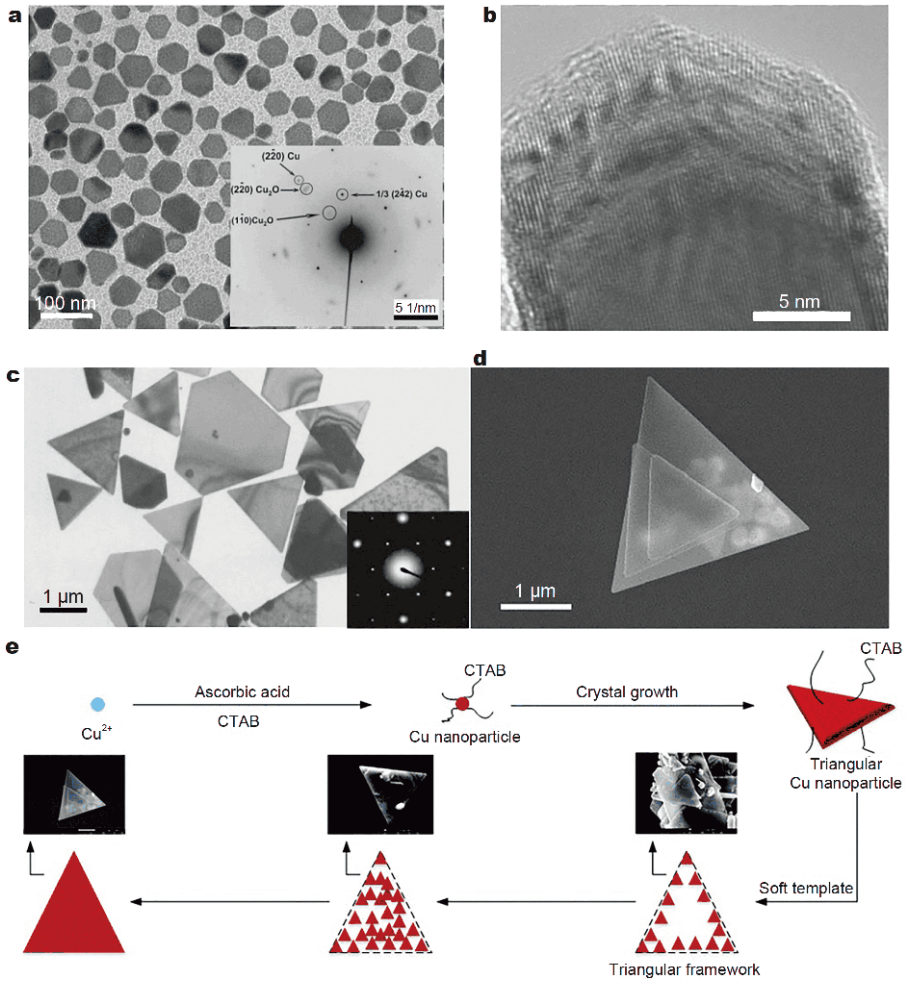

Figure 4 Synthesis of CuNFs. (a) Representative TEM image of CuNFs made by hydrazine reduction in dimethylformamide using PVP as stabilizer with an inset of the selected-area electron diffraction (SAED) pattern, and (b) HRTEM image of a single CuNF lying parallel to the TEM grid. Reprinted with permission from Ref. [78]. Copyright 2009, Wiley-VCH. (c) TEM image of CuNFs. Inset: the SAED pattern of an individual CuNF by reducing Cu^{+} with ascorbic acid in the presence of CTAB. Reprinted with permission from Ref. [77]. Copyright 2010, Elsevier. (d) SEM image of the products synthesized at CTAB concentration of 0.06 mol L^{-1} and pH 7. (e) The diagram of growth mechanism of CuNFs. (d, e) Reprinted with permission from Ref. [79]. Copyright 2017, the Royal Society of Chemistry.

formation of final morphologies of Cu nanomaterials. For example, the long chain alkylamine capping agents usually lead to large aspect ratio NWs for their selective adsorption to the five side {100} facets, resulting in ultralong penta-twined NWs. In comparison, PVP and CTAB are the surfactants for the synthesis of NFs as they can be adsorbed onto the special facets during the growth.

APPROACHES FOR THE ASSEMBLY OF COPPER NANOMATERIALS FOR SOFT CONDUCTORS

Copper nanomaterials are required to be incorporated into thin films to serve as soft conductors in various "skin-inspired" electronic devices [80,81]. There are typically two architectures ubiquitously adopted in a copper-based soft conductor: (1) the layered structure comprising a layer of conductive Cu nanomaterials and a layer of soft polymeric substrate [17,82,83]; (2) the bulk heterostructure containing a mixture of Cu nanomaterials and polymeric matrices [59,84]. In order to make these composites, solution-based assembly is used as a cost-effective technique, which does not require expensive equipment or vacuum conditions. In these processes, copper nanomaterials are dispersed in aqueous or organic solvents in the presence of polymers and molecular additives before the assembly procedure. In this part, we present and compare various assembly approaches used for copper-based soft conductors, including spray coat-

ing, spin coating, vacuum assisted assembly and transfer, drop casting, doctor blade coating, screen printing and controlled ink patterning. These approaches can control the film thickness from tens of nanometers to several micrometers with the fine tuning of deposition conditions and the selection of different sized Cu nanomaterials.

Spray coating

Spray coating is an assemly process in which aqueous or organic inks are atomized into uniform and fine droplets through a spray gun by means of moderately high pressure before reaching the to-be-coated substrate surface, which usually maintains a certain temperature to allow the deposited droplets to solidify into a thin film by quickly removing the solvent [85–93]. The ink preparation is therefore important to allow a uniform deposition of copper nanomaterial assemblies. Solvents, such as isopropanol (IPA), ethanol, hexane, or toluene, are used to improve the dispersion stability [63,85,89–94]. The Cu content can range from 0.6 to 1.2 mg mL^{-1} in the inks [91]. Fig. 5a illustrates a typical spray coating process to form CuNWs networks on a soft polyurethane (PU) substrate. The Cu inks were prepared by dispersing the as-prepared CuNWs in IPA. The accepting PU substrate was fixed on a rigid donor glass to avoid being deformed during the fabrication process. The Cu inks were then sprayed through a nozzle powered by an air compressor onto the PU substrate at a hotplate temperature of 60°C to ensure a uniform CuNWs tangled network. In order to improve the conductivity, the CuNWs network was annealed by photonic sintering, and the composite was peeled off from the glass substrate to attain a freestanding soft conductor [88]. It should be noted that, despite the easiness of spray coating to form desired conductive networks, its usage may still be limited by the substantial waste during the spraying process, the non-uniformity due to the uneven droplet evaporation, and the low resolution patterning restricted by the shadow masks [81,85,86].

Spin coating

Spin coating is a popular and convenient solution-based assembly method for the uniform thin film preparation [96]. In this approach, Cu inks are spread on a rotating substrate under the centrifugal force and form a solid thin film with the evaporation of the solvent. The thickness of the deposited thin film depends on solution viscosity, rotation speed and rotation duration. Before spinning, the surface of the substrate may be modified by a self-assembled monolayer of organic molecules to tune the hydrophobicity or hydrophilicity of the substrate, which would assist the formation of highly uniform films [83,97,98]. Other surface modification techniques, such as oxygen plasma, or UV ozone treatment may also facilitate the deposition of uniform thin films by turning the surface more hydrophilic. Typical Cu inks for the spin coating may involve the solvents of ethanol, and water [84]. Despite of the advantages of spinning coating, some drawbacks limit the process. One is that more than 90% of the initial solution is wasted during the rotation, and only a small portion can be used for the film formation. The limitation of the holder size is another drawback of spin coating. In addition, the process cannot produce designed patterns, unless additional lithography procedures are involved, which would increase the total fabrication cost [66,81].

Vacuum assisted assembly and transfer

Vacuum assisted assembly and transfer, also known as filtration and transfer, is a universal method to fabricate CuNWs thin mats on some flexible or stretchable substrates [52,65,99]. In a typical process (Fig. 5b), CuNWs are collected on a porous nitrocellulose, carbonylcellulose, polytetrafluoroethylene, or nylon membrances depending on the solvents under a pressure difference. The selective pores in the filtration membrane allow the removal of small CuNPs or insulating surfactants to render a more conductive network. In order to fabricate a soft conductor, the collected CuNWs are then carefully transferred onto a needed substrate, such as a sheet of PDMS, PU, PI, and poly(styrene-*b*-butadiene-*b*-styrene), by a contact transfer under a mild pressure from the filtration membranes [9,95,100–104]. Sometimes, a heat-tolerant releasing substrate, such as a glass slide, is used to receive the CuNWs before the eventual transfer to the polymeric substrate [82,100]. The purpose of two-step transfer is to allow the CuNWs thermally annealed in a reducing environment at a high temperature to remove the oxides. The polymer precursors, such as urethane liquid compounds, are then drop-casted or spin-coated onto the CuNWs (Fig. 5c). The curing of polymers enables an easily peelable elastomeric polymer/CuNWs layerd composite on the glass substrate [82]. In addition, the accompanied high roughness during the transfer may be eased by spin-coating another polymer layers (Fig. 5d), such as polymethyl methacrylate (PMMA) and poly(3,4-ethylenedioxythiophene) polystyrene sulfonate (PEDOT:PSS), to make a smooth conductive layer integrateable to LEDs or solar cells [17].

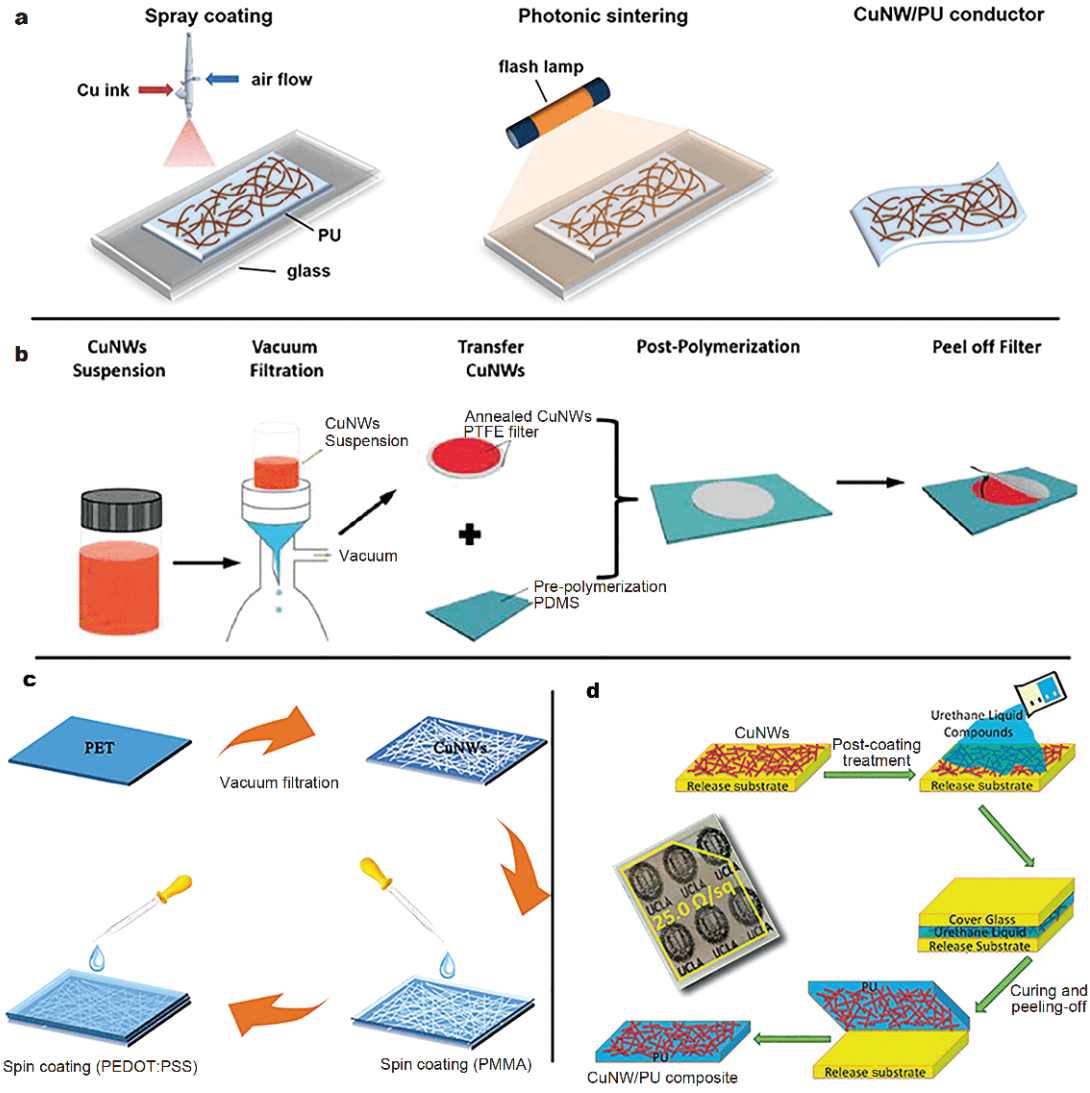

Figure 5 Spray coating and vacuum assisted assembly and transfer for copper-based soft conductor. (a) Schematic illustration of the fabrication process of CuNWs/PU conductors. The Cu ink was sprayed onto the PU substrate that fixed on rigid supporting glasses through a nozzle powered by an air compressor, followed by photonic sintering treatment to obtain conductive networks. The CuNWs/PU conductors were prepared by carefully peeled off from the glass substrate. Reprinted with permission from Ref. [88]. Copyright 2016, American Chemical Society. (b) Schematic of the fabrication process of CuNWs/PDMS. CuNWs were collected on PTFE filters through vacuum filtration, which were carefully transferred onto the slightly sticky PDMS substrate and followed by post polymerization. The CuNWs/PDMS composite films were obtained by peeling off from the filters. Reprinted with permission from Ref. [95]. Copyright 2016, American Chemical Society. (c) Schematic illustration of the fabrication process of a CuNWs-PU composite electrode. Reprinted with permission from Ref. [82]. Copyright 2014, the Royal Society of Chemistry. (d) Schematic of the fabrication process of CuNWs/PMMA/PEDOT:PSS. Reprinted with permission from Ref. [17]. Copyright 2019, Nature Publication Group.

Doctor blade coating

Doctor blade coating is a conventional thin film deposition technique, in which a sharp blade moves over the Cu inks on a substrate, leaving a thin film of Cu composites with a uniform thickness, which is controlled by the gap distance between the blade and the substrate [49,105]. Doctor blades can be replaced by Mayer rods, i.e., periodical grooved rods or wire-wound rods, to control the thickness of thin films by the groove or wire geometries [81,106,107]. Inks are squeezed through the empty spaces from the grooves or wires to form uniform thin films. Soft conductors based on CuNWs have been coated on the PET substrate using a Meyer rod [49] (Fig. 6a, b). CuNWs inks suitable for this coating method have a relatively high viscosity, faciliated by nitrocellulose added in a cosolvent of acetone, ethanol, ethyl acetate, pentyl

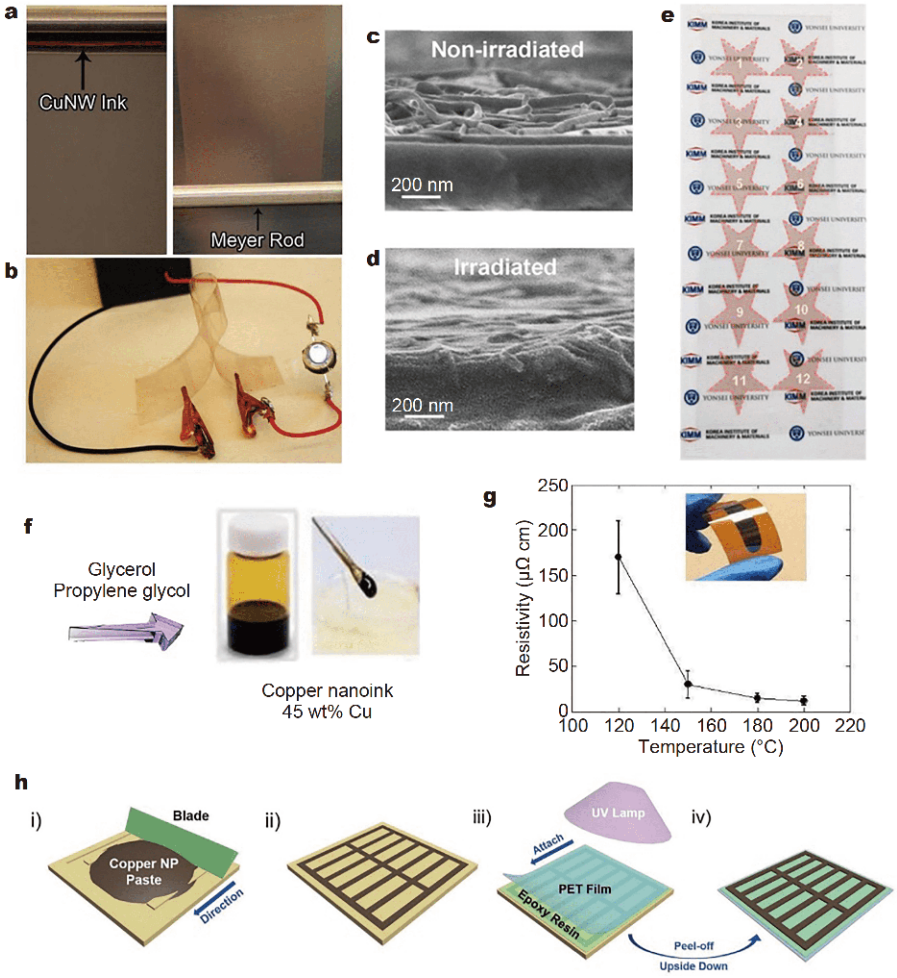

Figure 6 Doctor blade coating and screen printing for copper-based soft conductors. (a) Conductive flexible film with CuNWs assemblied on the PET with a Meyer rod. (b) The CuNWs film in a bending state. Reprinted with permission from Ref. [49]. Copyright 2011, Wiley-VCH. SEM images of the cross section of CuNWs-coated areas with (c) and without (d) intense pulsed light irradiation. (e) Photograph of the 12-star-patterned CuNWs on a polycarbonate substrate after the intense pulsed light irradiation and wiping process. (c–e) Reprinted with permission from Ref. [106]. Copyright 2016, American Chemical Society. (f) Schematic illustration of the prepared 1-amino-2-propanol (AmIP) capping CuNPs dispersing in the glycerol and propylene glycol blending ink. (g) Electrical resistivity of Cu film after the thermal sintering of Cu nanoink on PI film for 15 min at 120, 150, 180, and 200°C. Reprinted with permission from Ref. [108]. Copyright 2015, American Chemical Society. (h) Schematic illustration of the CuNPs patterning and transfer to the flexible substrate. i), ii) CuNPs paste is uniformly filled in the trench of Si master mold and excessive NPs are removed by a doctor blade method. iii) The UV-curable epoxy resin spin-coated and a PET substrate placed onto the epoxy resin. The epoxy is hardened under UV lamp irradiation to promote the adhesion. iv) A film of copper/epoxy/PET is peeled-off from the master mold. Reprinted with permission from Ref. [109]. Copyright 2017, Wiley-VCH.

acetate, IPA, and tolunene [49]. Vortex mixing was used to make the inks more homogenous, and the final concentration of CuNWs was approximately 8 mg mL^{-1} [49]. In a different example, PVP capped CuNWs were dispersed in IPA to the concentration of 0.5 wt% to form suitable inks, which were coated on a polycarbonate substrate to form 80–100 nm thick CuNWs films by a Mayer rod [106]. The CuNWs were fused with each other and embedded into the substrate at the nanoscale level by intense pulsed light sintering (Fig. 6c, d), and the un-irradiated area was removed by a wiping fabric soaked with the IPA solvent (Fig. 6e). CuNPs inks capable for doctor blade coating have been prepared by dispersing 1-amino-2-propanol (AmIP) capping CuNPs in the glycerol and propylene glycol with a concentration of 45 wt% Cu [108] (Fig. 6f). The resistivity of the coated CuNPs films reached 30 μΩ cm after a thermal treatment at 150°C in nitrogen (Fig. 6g).

Screen printing

When a patterned screen is used as a mask in the doctor blading process, this process is evolved into screen printing, which allows the ink to penetrate through the open windows of the screen onto the target substrate [13,109–112]. The screens are made from photo-lithographically patterned fabrics or etched stainless steels or even silicon wafers [81,113]. The screen can be away from the substrate below for a controlled distance to allow a clean transfer of the inks. The inks usually have a high viscosity to prevent the leakages across the porous openings [81,112]. Fig. 6h shows a practical example of CuNPs patterning and transfer to the flexible substrate by means of screen printing. The CuNPs high-viscosity paste was uniformly filled in the trench of Si master mold and excessive NPs were removed by a doctor blade, and then UV-curable epoxy resin was spin-coated before a PET foil was placed on top. The film of copper/epoxy/PET was peeled off from the master mold into a soft conductor after the epoxy was hardened under UV irradiation [109].

Controlled ink patterning

There are three typical printing types for controlled ink patterning of Cu inks: inkjet printing, direct-write printing, and ball-pen printing. The formulations of inks are important for these assembly methods, as "coffee-fringe" or central "mountaintop" effects tend to occur, resulting in uneven surface, if the ink volatility and viscosity are not precisely controlled. Therefore, the preparation of the ink is crucial to the quality of the patterns fabricated by ink printing.

Inkjet printing is an attractive assembly technique for patterning various materials into arbitrary microscale patterns. The inks, consisting of well-dispersed nanomaterials in homogeneous solvents, are ejected by a piezoelectric device as tiny microscale droplets (Fig. 7a), which are directly deposited on the designated places on the substrate [114–124]. In a typical example, a suitable ink was obtained by dispersing the CuNPs in a mixture of 2-amino-2-methyl-1-propanol and distilled water at pH 9 with a wetting agent at a concentration of 0.1 wt%. A commercial office inkjet printer was used to print the inks into a functional radio frequency identification antenna [115] (Fig. 7b). The printed lines composed of closely packed NPs were about 300 μm in width and 400 nm in thickness [115]. These CuNPs could be inkjet-printed to yield a conductive and decorative pattern (Fig. 7c) [115].

Direct-write printing, also referred as three-dimensional (3D) additive printing if layer-by-layer deposition is involved, is an assembly method for digitally controlled deposition of a viscoelastic ink extruded from a small nozzle [125,127–132]. Complex metallic architectures can be fabricated through direct-write printing of CuO inks with a subsequent thermochemical transformation into sintered metallic counterparts [125]. The viscoelastic CuO inks were prepared by mixing the CuO powder, tri-solvent mixture (dichloromethane, dibutyl phthalate and 2-butoxyethanol) and the appropriate volume of biomedical elastomer (polylactic-*co*-glycolic acid) (Fig. 7d). The inks were 3D-printed under ambient conditions *via* simple extrusion at speeds upwards of 150 mm s^{-1} into a centimeter-scale hollow and enclosed CuO box (Fig. 7e). The as-printed architectures were transformed into copper counterparts without cracking or warping through thermochemical reduction and sintering in a H_2 atmosphere at elevated temperature of 300–600°C (Fig. 7f) [125].

Ball-pen printing is a technique to print the Cu inks using a conventional ball pen into desired conductive patterns. Using the metal ball at the tip, the ball pen dispenses high-viscosity Cu inks at the manually or digitally controlled locations. The Cu inks suitable for this approach have been obtained by dispersing the as-synthesized CuNWs in deionized water with the assistance of hydroxypropyl cellulose (HPC) (Fig. 7g). The inks were filled into a ball pen (Fig. 7h) and were applied to various flexible substrates. A hand-drawn conductive pattern following the image of Sydney Opera House (Fig. 7i) easily lighted an LED light. The electrical current flowing through the conductive lines changed little after 3000 cycles at a stretching strain of 10% [126].

INTRINSIC PHYSICAL PROPERTIES OF COPPER NANOMATERIALS

Soft electronics typically require the macroscopic assemblies of copper nanomaterials as the required electronic components. Despite this fact, understanding the intrinsic electrical properties (conductivity, current carrying capacity, etc.), mechanical properties (elongation at break, elastic modulus, stiffness, etc.) and dynamic performance (stretching resistance, bending resistance, etc.) of the individual copper nanomaterial is equally important. Due to the high aspect ratios of CuNWs, their physical properties are easier to be investigated in comparison to those of the 0D and 2D counterparts. In this section, we review the studies of the electrical and mechanical properties of individual CuNWs.

The electrical properties of a single CuNW synthesized by solution-based process using glucose and HDA were characterized by a two-probe method, in which a 14 μm

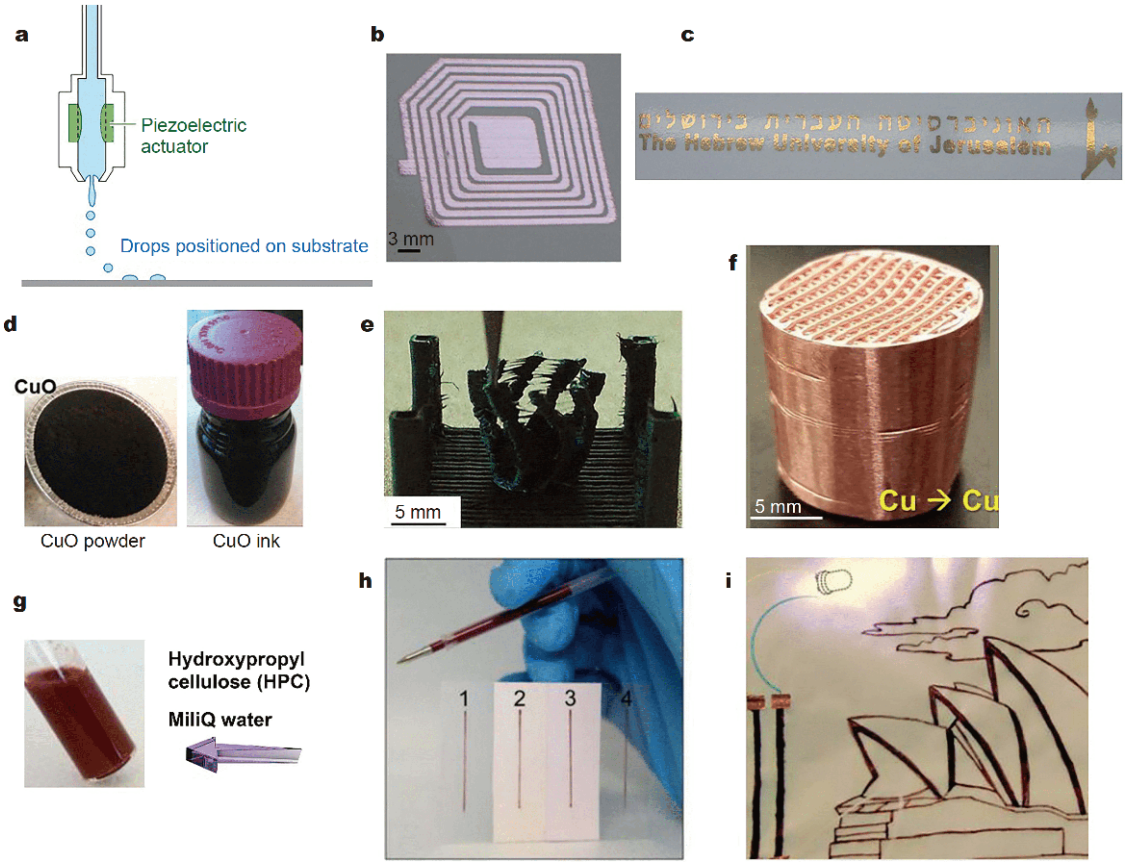

Figure 7 Controlled ink patterning for copper-based soft conductors. (a) Schematic illustration of the operation of a drop-on-demand inkjet system. Reprinted with permission from Ref. [114]. Copyright 2010, Annual Reviews. (b) An antenna printed on a paper by the means of inkjet printing. (c) Decorative inkjet printing of a 5 wt% dispersion of Cu/Ag core-shell NPs on an inkjet photo paper with the use of a Lexmark office printer. (b, c) Reprinted with permission from Ref. [115]. Copyright 2009, the Royal Society of Chemistry. (d) CuO inks used for 3D printing are produced by combining the CuO powders with the tri-solvent mixture (dichloromethane, dibutyl phthalate and 2-butoxyethanol) containing the appropriate volume of the dissolved elastomer, polylactic-*co*-glycolic acid. (e) Photo of the initial progress of 3D-printing of a CuO box. (f) Photograph of copper structures resulting from thermally processed cylinder 3D-printed from CuO inks. (d–f) Reprinted with permission from Ref. [125]. Copyright 2015, Wiley-VCH. (g) Optical image of the CuNWs ink, in which CuNWs suspended in MiliQ water with the help of the stablizer HPC. (h) CuNWs in a ball-pen refill and writing ink traces on different substrates. (i) Painted conductive image of Sydney Opera House using CuNWs ink. (g–i) Reprinted with permission from Ref. [126]. Copyright 2015, American Chemical Society.

long CuNW with a diameter of 200 nm was bridged between two Ti/Au electrodes (Fig. 8a). In order to reduce the contact resistance by eliminating the effect of oxide on the CuNWs, focused ion beam milling and Pt deposition were conducted on the two ends of the contact. In this way, contact resistance was reduced to as little as 9 Ω. The current-voltage (*I*-*V*) curve of the CuNW was linear at the low bias, and became non-linear when the Joule heating increased the resistance of the CuNW (Fig. 8b). The conductivity of a single CuNW was then estimated to be 3.4×10^5 S cm^{-1}, slightly smaller than the value of 5.9×10^5 S cm^{-1} for bulk Cu, which indicated that the planar defects such as twinning and stacking faults were not significantly detrimental to the electrical conductivity. The CuNW broke down at a maximum current density or ampacity of 3.8×10^7 A cm^{-2}, which was more than an order of magnitude higher than that of the bulk Cu (Fig. 8b). In addition, the electromigration effect in the direction of anode electrode was observed on the CuNW at high current densities (Fig. 8a), when the electron wind transferred the Cu atoms along the length of the CuNW [133].

The mechanical properties of CuNWs are dependent on the sample sizes, which are confirmed by the uniaxial *in situ* tensile tests on crystalline CuNWs in a TEM chamber [134]. The single-crystalline CuNW with a diameter of ~5.8 nm had an exceedingly large recoverable strain up to 7.2% (Fig. 8c), which was observed in the

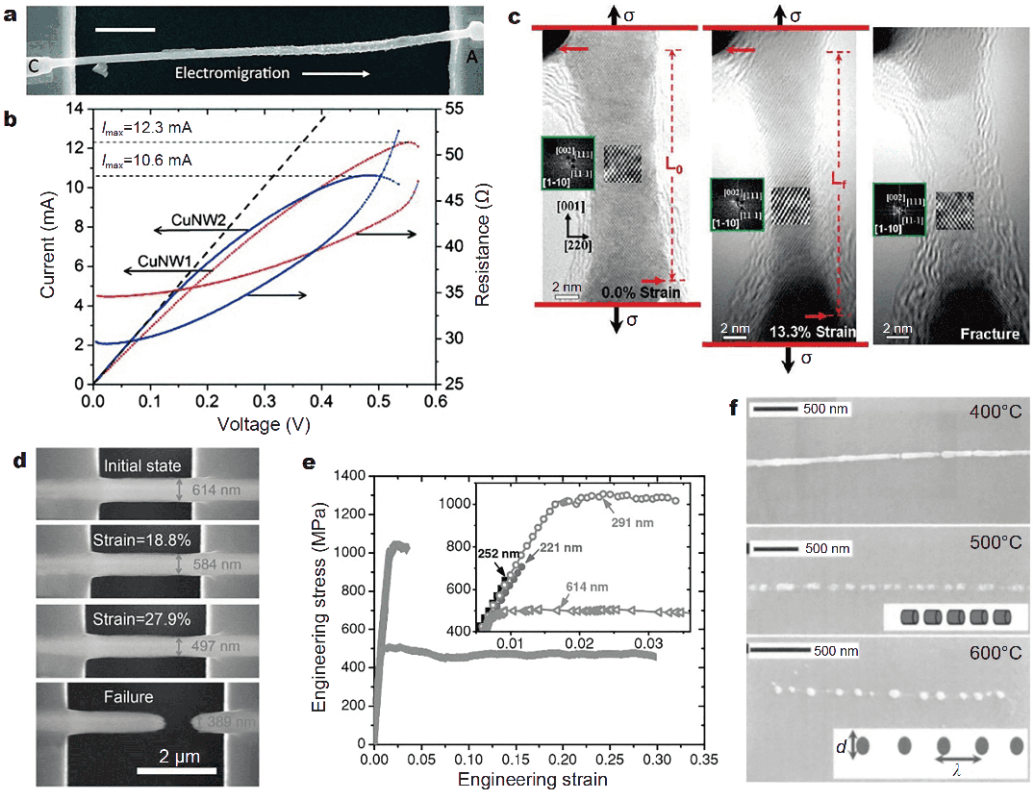

Figure 8 Intrinsic physical properties of copper nanomaterials. (a) SEM of the device for electrical measurement. A large current has passed through the CuNW wire. Scale bar is 2 μm. The anode and cathode are labelled A and C respectively. It shows the effect of electromigration. Electromigration is in the direction of the anode electrode. (b) *I-V* curves and the corresponding resistance of the CuNW1 and CuNW2. I_{max} is the maximum current passing through the CuNW. (a, b) Reprinted with permission from Ref. [133]. Copyright 2017, the Royal Society of Chemistry. (c) *In situ* atomic-scale deformation process of a singlecrystalline CuNW at different total strains conducted in the TEM chamber from 0% strain to 13.3% strain and after fracture. The insets are the corresponding FFT images of panels. Reprinted with permission from Ref. [134]. Copyright 2011, American Chemical Society. (d) *In-situ* observation of a CuNW during tensile deformation investigated in an SEM chamber. (e) Four representative engineering stress-strain plots for CuNWs of varying sizes. (d, e) Reprinted with permission from Ref. [135]. Copyright 2012, Wiley-VCH. (f) Rayleigh instability of the CuNWs displayed by SEM micrographs of CuNWs after annealing at 400, 500 and 600°C. CuNWs show different degrees of fragmentation into a chain of long cylindrical sections or nanospheres along their axes. The insets represent schemes of the corresponding fragment geometries. Reprinted with permission from Ref. [136]. Copyright 2004, AIP Publishing.

atomic-resolution scale, consistent with the predictions from molecular dynamics simulations and approaching the theoretical elastic strain limit. In addition, the maximum elastic strain would decrease with the increase of the sample diameter [134]. Fracture strengths for single-crystalline CuNWs with diameters ranging from 131 to 655 nm were investigated in a micromechanical device in an SEM chamber (Fig. 8d). It was found that the fracture strengths of CuNWs were much higher than that of bulk copper, reaching 400 to 1000 MPa depending on the CuNWs diameters [135] (Fig. 8e). Both ductile and brittle behavior occurred, which was related to the density of defects at the initial state and the subsequent dislocations of atoms during the uniaxial stretching. A higher fracture strength of 7 GPa was found for CuNWs with diameter of 75 nm [137]. In addition, the Rayleigh instability of CuNWs has been systematically investigated [136]. Different stages of the fragmentation process would occur when CuNWs were annealed with diameters of 30–50 nm at temperatures between 400 and 600°C. The CuNWs started to fragment at 400°C, which was far below the melting point of bulk Cu (1083°C), and formed shorter sections at 500°C, and then decayed into a chain of nanospheres at 600°C (Fig. 8f). Rayleigh instability of CuNWs should be considered during the thermal treatment of CuNWs networks [136].

ANTIOXIDATION STRATEGIES FOR COPPER-BASED SOFT CONDUCTORS

A well-known disadvantage of copper nanomaterials is

their intrinsic tendency to oxidize, therefore limiting their applications in soft electronics. How to improve the stability of copper nanomaterials is an area of particular interest for practical applications.

The stability of CuNWs and their oxidation kinetics in various liquids have been studied and compared [138]. The "dangling" bonds on the surface of the as-synthesized CuNWs are extremely sensitive to the external environment giving the CuNWs high reactivity and poor stability. The stability of CuNWs in the liquid phase was evaluated by monitoring the change of morphology, phase, and valence state of CuNWs during storage. It was found that the CuNWs produced by the hydrazine reduction method [51] exhibited durable chemical stability and dispersibility in polar organic solvents but evolved into mace-like structures when stored in water or nonpolar organic solvents. EDA molecules dangling on the surfaces of CuNWs were of great significance in the dispersibility of CuNWs in polar solvents. Moreover, the final morphology, phase, optical absorption, band gap properties of the oxidation products were dependent on the different oxidation pathways. For example, heating fresh CuNWs in air can result in thin shells of CuO. CuNWs with EDA capping agents stored in water or nonpolar organic solvents are highly sensitive to oxygen and evolve into a heavily-oxidized mace-like structure, while the oxidation is prevented in polar organic solvents. The oxidation might be avoided by adding suitable reductants during storage. However, slight oxidation of CuNWs on the surface is usually inevitable, which should be considered in the future practical applications.

To date, several reasonable strategies have been suggested to address the stability issue of copper nanomaterials. One is to introduce antioxidant alloyed encapsulation layers made of Au, Ag, Pt, Ni on the surface of individual Cu nanomaterials [34,70,139–141]. The second approach is to immerse Cu nanomaterials in polymeric matrices or between two airtight layers such as PDMS, PU, poly(vinyl alcohol) (PVA) to improve the antioxidation ability [82,142]. The third attempt is to cover individual Cu nanomaterials with a thin organic or inorganic monolayer, such as self-assembled molecules or graphene to improve the oxidation stability [54,60,89].

Metal protection

The reactive surface of Cu nanomaterials may be protected by more inert metal layers by various chemical or electrochemical means to form core-shell structures [140]. This strategy leaves few sites for oxygen or water to attack the interior atoms, therefore enhancing the stability [143–145].

Nobel metals, such as Au, Ag and Pt, can form effective protection layers to prevent Cu from oxidation [140,146]. Ag is especially favored due to the lower cost in comparison to Au and Pt [34,70,141], although it might be oxidized with long time exposure to air or be eroded in a more reactive environment [5]. There are several ways to uniformly coat Cu nanomaterials with an Ag layer [140]. Considering that Ag has a higher reduction potential than Cu, Ag ions can react with Cu to form the Ag layer by the galvanic replacement reaction [147–149]. Cu@Ag NPs were obtained by reacting CuNPs obtained in oleylamine with $AgNO_3$ at a reaction temperature of 80°C (Fig. 9a, b). The alloyed NPs were stable for at least a month, and no oxidation was observed using X-ray photoelectron spectroscopy (XPS) [149]. Ag coated CuNWs have been obtained in a similar way by reacting the CuNWs with $AgNO_3$ at room temperature. However, the galvanic replacement can lead to the fracturing of CuNWs or hollow structures due to the oxidation attack of Ag^+. Therefore, electroless deposition is chosen as an alternative way to coat Ag layer on copper. To avoid the galvanic displacement, ascorbic acid was introduced to reduce Ag^+ without affecting Cu, therefore creating Ag layer on Cu. Other less oxidizing Ag salts, such as Ag-amine complexes, have been shown to effectively create the core-shell structure without inducing the galvanic replacement reaction. Ag-amine complexes adsorbed onto the Cu surface would be decomposed into pure Ag after annealing at 140°C for 5 min [34]. In addition, Ag can be directly electroplated to the CuNWs networks in a roll-to-roll continuous way. In this process, the Ag coating can be systematically controlled by changing the current density and the electroplating time [141].

Other than Ag, Ni is a much less expensive alternative to serve as a protective metal. Ni has been directly coated on the CuNWs in an electroless deposition solution containing PVP, ethylene glycol, $Ni(NO_3)_2$, and N_2H_4 at 120°C [150]. The thickness of Ni layer was controlled by the initial molar ratios of Cu to Ni ions, and the diameter of CuNWs increased from 75 to 116 nm after they were coated with Ni when the Ni concentration was estimated to be 54% [150]. The external layer of Ni was obvious in the EDS image (Fig. 9c) [150]. With the assistance of Pd ions, the temperature needed for the electroless deposition of Ni was reduced to 75°C [140]. Ni coating was found to effectively prevent Cu from oxidation. At a humidity of 85% and a temperature of 85°C, thin films made of CuNWs and even AgNWs showed significant degradation, while those made of Ni coated CuNWs had

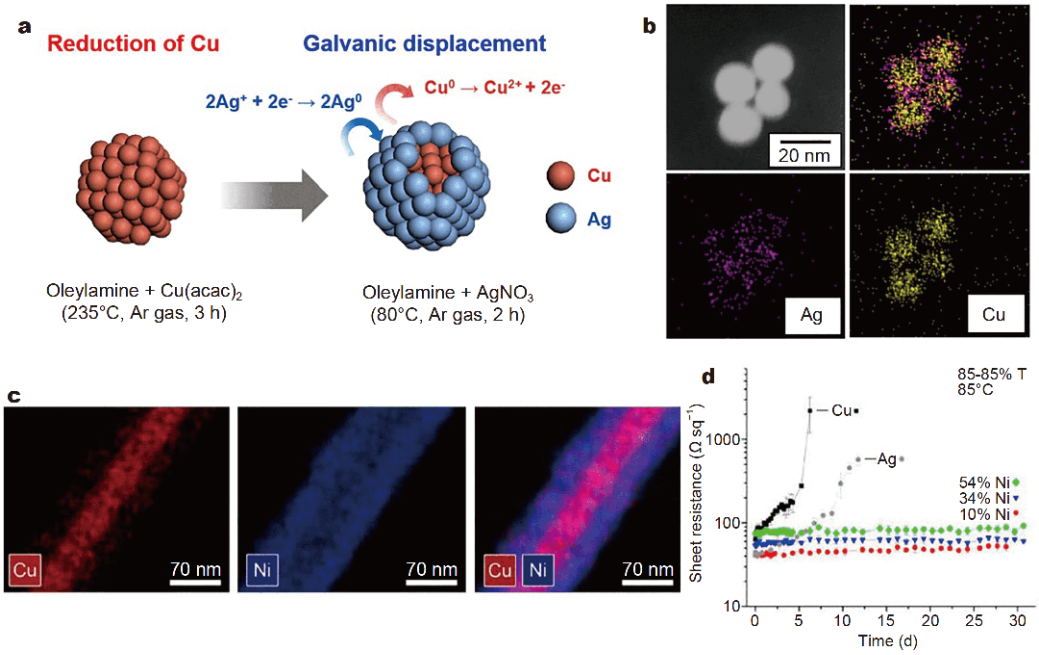

Figure 9 Antioxidation by metal protection. (a) Schematic representation of the synthesis of Cu@Ag core-shell NPs. (b) EDS elemental mapping analysis of the NPs. (a, b) Reprinted with permission from Ref. [149]. Copyright 2015, IOP Publishing. (c) EDS images of a CuNW coated with 54 mol% nickel. (d) Plot of sheet resistance *versus* time for films of AgNWs, CuNWs, and cupronickel NWs stored at 85°C. Reprinted with permission from Ref. [150]. Copyright 2012, American Chemical Society.

a quite stable electrical properties even when the Ni content was only 10% [150] (Fig. 9d). Ni-Cu alloyed NWs have been synthesized by a scalable one-pot method, in which the Cu and Ni precursors were reduced together in oleylamine at 180°C for 4 h, and at 205°C for another hour. At 180°C, Ni ions mainly served as a catalyst, therefore yielding CuNWs only, and were further reduced at higher temperatures by oleylamine into Ni-Cu alloyed NWs. The soft conductors made from these alloyed NWs demonstrated almost unchanged resistance within 30 d [102]. A more obvious Ni shell was observed when Ni precursors were added in a later step after CuNWs were formed in the HDA-CTAB melts at 210°C, and these Ni coated CuNWs showed improved stability [139].

Polymer matrices

Polymers, such as PDMS or PI, are widely used as an encapsulation layer for electronic devices and integrated circuits. When Cu nanomaterials are embedded in polymer matrices, the polymers serve as a protection layer to avoid the direct contact of Cu in air, and thus an enhanced stability has been observed [82,142]. However, the polymers might not stop the permeation of moisture or air completely, and therefore may not completely prevent the oxidation of Cu. In order to solve this problem, an inorganic SiO_x layer was used to overcome the drawback of the polymer [142]. Fig. 10a demonstrates the flexible film structure that uses PI and SiO_x layers to prevent the oxidation of CuNWs. A PI/SiO_x/PI triple layer structure was used to stop moisture and oxygen, and increase the abrasion resistance of the coating. Resistance changes of the CuNWs/PI/SiO_x/PI were measured under extreme conditions to check its antioxidation performance. It was found that the resistance changes of the CuNWs/PI/SiO_x/PI composite samples were very small when compared with that of the CuNWs after they were exposed to water at room temperature for 7 weeks. There were no resistance changes or etched regions, when CuNWs/PI/SiO_x/PI samples were immersed in the copper etchant for 10 min.

Monolayer coatings

The oxidation of the active Cu atoms on the surface should be blocked if a dense monolayer coating is applied. Long chain alkylamine capping agents can form self-assembled monolayers on a Cu surface [54], which is expected to be an effective protective layer. Oleylamine is one type of typical ligands attached to Cu surfaces during the synthesis, but the molecules are usually not able to form an impenetrable layer due to the low binding energy

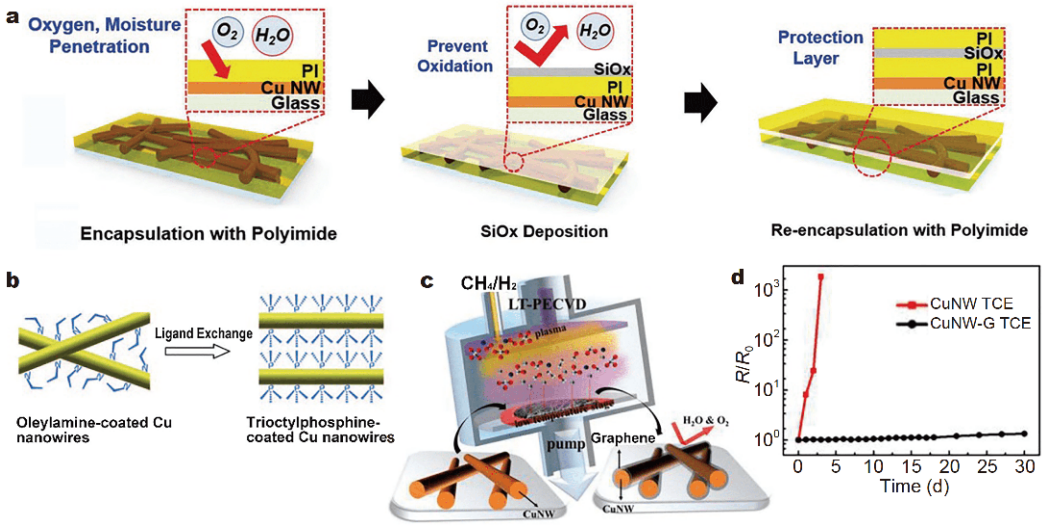

Figure 10 Antioxidation by polymer matrices and monolayer coatings. (a) Schematic illustration of the fabrication process of CuNWs/PI/SiO_x/PI composite film for antioxidation performance improvement of the CuNWs conductive film. Reprinted with permission from Ref. [142]. Copyright 2019, Wiley-VCH. (b) Schematic of the ligand exchange from oleylamine- to trioctylphosphine-coated CuNWs. Reprinted with permission from Ref. [60]. Copyright 2011, Wiley-VCH. (c) Schematic illustration for the low-temperature plasma-enhanced CVD (LT-PECVD) system for the synthesis of CuNW-G core-shell nanostructure construction. (d) Sheet resistance changes of CuNWs and CuNW-G TCEs during a stability test in air at room temperature for 30 d. Reprinted with permission from Ref. [89]. Copyright 2015, American Chemical Society.

and large space between each adsorbed oleylamine molecule [60]. Therefore, CuNWs with attached oleylamine are not resistant to oxidation. It was reported that trioctylphosphine had a higher binding energy to Cu surfaces than oleylamine, and improved the surface stability of CuNWs after the ligand exchange (Fig. 10b). As a result, thin films made from trioctylphosphine coated CuNWs retained the metal luster after storage in air for two years, while the oleylamine-coated CuNWs gradually became tarnished during the storage [60]. The oxidation resistance of the EDA ligand in solution has also been investigated systematically. It was experimentally confirmed that EDA affected the oxidation state of the as-synthesized Cu surfaces. Density functional theory calculations revealed that EDA effectively blocked the adsorption of oxidizing species (OH^-) and the oxidation of Cu seeds, which was attributed to a filling of the antibonding states accompanied by an increase of the electrostatic repulsion [151].

Graphene endows the soft electronics with outstanding reliability and long-term stability as well as high conductivity [12,25,26,28,152]. Especially, graphene oxide or reduced graphene oxide can provide an effective monolayer for protecting the inner metal atoms from corrosion [153]. Copper nanomaterials were composited with a layer of graphene to effectively suppress the oxidation process. Fig. 10c shows the schematic illustration for the low-temperature plasma-enhanced chemical vapor deposition (CVD) system for the synthesis of CuNW-graphene core-shell nanostructure construction at a temperature as low as 400°C. Thin films made from CuNW-graphene were much more stable in air at room temperature in comparison to the uncoated ones within a testing period of more than 30 d (Fig. 10d) [89]. This remarkable oxidation stability was due to the tight encapsulation of the gas-impermeable graphene shells around the CuNWs. Solution-based fabrication of CuNWs/graphene core-shell structures was also demonstrated [32]. Graphene oxide nanosheets were wrapped onto the CuNWs surfaces by controlling the surface chemistry, and the colloidal composites were stable in a variety of polar solvents while stored in air [32]. Graphene oxide was partially reduced by a mild thermal annealing to enable high quality graphene covered CuNWs. The transparent conductors made from these core-shell NWs had been stable for 200 d in air [32].

APPLICATIONS

The progress in the research of copper-based composites is driven by their potential applications in the soft electronics by serving as a cost-effective replacement for expensive Au or Ag based counterparts. In this section, we summarize the recent advances of copper-based soft materials in the application of stretchable conductors, soft

transparent electrodes, solar cells, LEDs, electromechanical sensors, and wearable heaters. The summary tables for each Cu-based device applications are provided in the Supplementary information.

Stretchable conductors

The high aspect ratios of CuNWs allow the sliding of NW contacts during the stretching, making them potential candidates for stretchable conductors (Table S1). A high-performance stretchable conductor may show little change of resistance during stretching. A simple stretchable conductor was made by layering the network of CuNWs on an elastomeric PDMS substrate. Due to the fractures of CuNWs or the loss of connections, a nine-fold increase of resistance was observed at a strain of 30%, and almost 100-fold increase of resistance at a strain of 50% for the thin films of CuNWs on PDMS. The resistivity increased with repeated strain cycles, and stabilized after 20 cycles [92]. The resistance changes upon stretching became less sensitive when the CuNWs were welded at the nanoscale junctions by a circularly polarized laser [99]. The laser-nanowelded CuNWs networks on PDMS (Ecoflex) endured very large strain up to 250% without substantial cracks and resistance increase (Fig. 11a). In comparison, the as-prepared CuNWs exhibited obvious cracks and fast degradation of con-

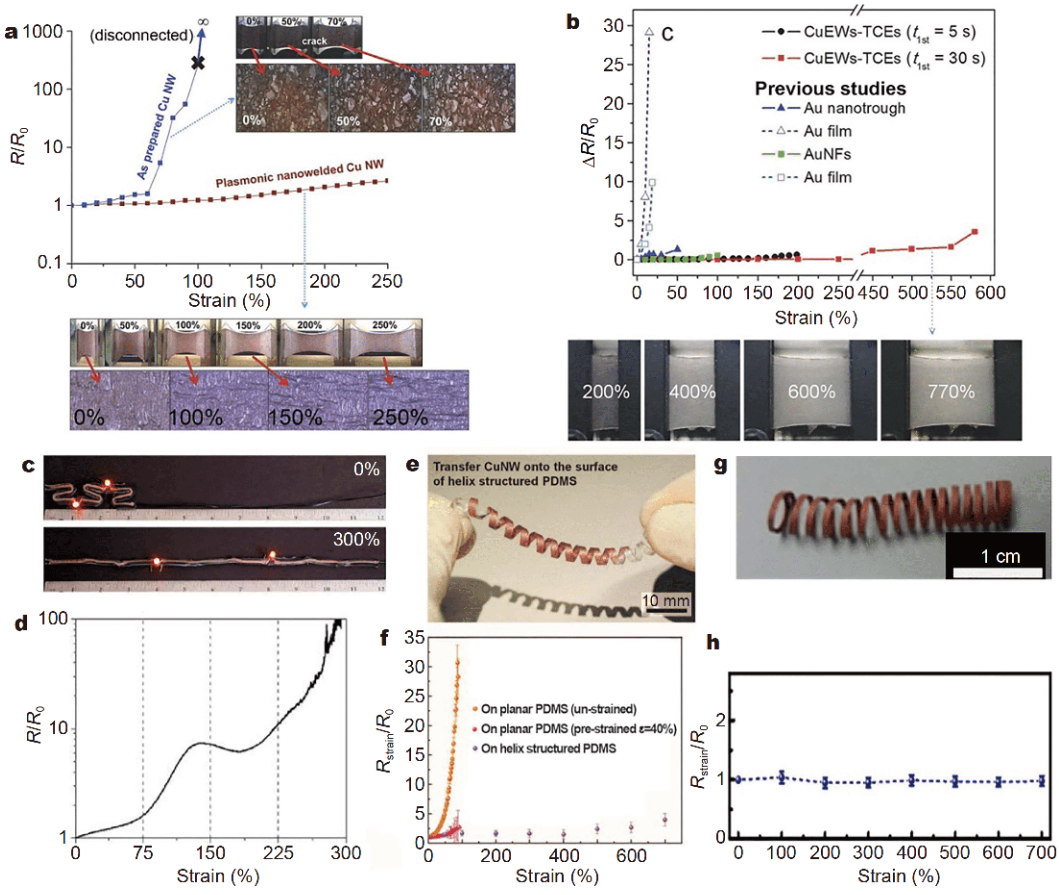

Figure 11 Copper-based stretchable conductors. (a) Stretchability test of the as-prepared CuNWs conductor and the plasmonic nanoweled CuNWs conductor with their corresponding photographs and optical microscopy images. Reprinted with permission from Ref. [99]. Copyright 2014, Wiley-VCH. (b) Uniaxial strain in tensile test of Cu electroplated NW meshes for TCEs on PDMS (Ecoflex) compared with some results of the previous studies with insets of the photo images during stretching up to 770%. Reprinted with permission from Ref. [67]. Copyright 2016, Wiley-VCH. (c) A serpentine variant of stretchable Cu-AgNWs conductors with LEDs circuit at 0% and 300% strain. (d) Strain *vs.* R/R_0 behavior of the serpentine Cu-AgNWs trace at various degrees of strain. Reprinted with permission from Ref. [154]. Copyright 2018, American Chemical Society. (e) Photograph of the fabricated helical-structured CuNWs electrode. (f) Relative resistance variation as a function of strain for stretchable CuNWs electrodes fabricated on the planar and the helical-structured PDMS substrates, respectively. Reprinted with permission from Ref. [155]. Copyright 2014, Nature Publication Group. (g) Helical-shape Cu stretchable conductor electroless deposited on PDMS, and (h) the normalized resistance of the Cu-PDMS stretchable conductor under different tensile strains. Reprinted with permission from Ref. [83]. Copyright 2018, American Chemical Society.

ductance even within the strains smaller than 100% (Fig. 11a) [99]. Similarly, the self-welding of CuNWs by electrospinning and electroplating led to stretchable networks with less than 5-fold increase in resistance when stretched by 580% (Fig. 11b) [67].

Instead of direct layering, elastomers can infiltrate into CuNWs networks or felts to fabricate a stretchable composite. A typical CuNWs felts have a porosity of 90.5%, allowing the elastomers to penetrate through [154]. The conductivity of the composite reached 1220 S cm^{-1}, only 47 times less conductive than bulk Cu at the similar porosity. The resistance-strain behavior was dependent on the mechanical properties of PDMS [154]. The composite with less stiff PDMS (Ecoflex) exhibited an increase of resistance by 12%, 52%, and 146% at strains of 50%, 100%, and 150% respectively [154]. The composites with stiffer PDMS (Dragon Skin) exhibited much higher increase of resistance at similar strains [154]. The presence of the elastomer matrices was believed to prevent the fracture and breakup of the CuNWs felts, thus facilitating the improved stretching performance [154].

Despite the enhanced stretchability conferred by these strategies, the intrinsic stiffness of the copper nanomaterials often results in electrical failure before the mechanical failure of the flexible conductors owing to the strain-induced microcracking and disconnections of the copper nanomaterials. Some mechanical structures, such as serpentine shapes [154] and helical shapes [83,155], can effectively dissipate the strain induced in the flexible conductors and enhance their stretchability. Fig. 11c shows a serpentine variant of stretchable Ag coated CuNWs conductors, making the conductors workable at a strain of 300%. The resistance change of the serpentine conductor at different strains is shown in Fig. 11d [154]. CuNWs thin films were able to be transferred to helical surfaces (Fig. 11e), leading to a helical conductor with a stretchability of 700% with no significant change of resistance. This mechanical/electrical performance was much better than that of CuNW films transferred to the unstrained or pretrained PDMS substrates (Fig. 11f) [155]. Fig. 11g demonstrates a similar helical-structured Cu conductor, in which the Cu was electrolessly deposited on PDMS [83]. This conductor also reached a maximum strain of 700% with nearly no resistance change (Fig. 11g).

Soft transparent electrodes

Next-generation optical electronics require cost-effective, lightweight, flexible and scalable transparent conductors [156]. Indium tin oxide (ITO) has been used as the transparent conductors in most devices due to its high conductivity and transmittance. However, the major limitations of ITO for the use in next-generation soft electronics are its brittleness, scarcity and rising costs [49,70,157]. Due to the flexibility of copper nanomaterials, especially CuNWs, their thin films are the potential candidates to replace ITO in various optical electronics [49,60,158] (Table S2).

A great transparent conductor is characterized by a good balance of transmittance and conductance. To achieve this goal, the thickness of CuNWs thin films was finely tuned by controlling the volume of CuNWs dispersions. The films exhibited great transparency at wavelengths from 350 to 1700 nm, and the transmittance became lower with increased thickness or loading of CuNWs (Fig. 12a, b) [65]. A comparison of CuNWs thin films with ITO and other candidates, such as AgNWs, graphene, and carbon nanotubes confirms that they can reach a similar conductivity and transmittance performance but at a much lower cost (Fig. 12c) [49]. The optical haze of CuNWs thin films, relating to the scattering of light, is also an important factor characterizing the quality of a transparent conductor. It was found that the haze factor was only about 2%–3% at the transmittance of 90% when 17.5 nm CuNWs were used to minimize the light scattering [65]. In addition, CuNWs transparent conductors with a sheet resistance of 40 Ω sq^{-1} had a maximum current carrying capacity of about 533 mA cm^{-2} [49]. The ability to carry large currents for CuNWs thin films is an attractive feature for them to be applied in photovoltaics or LEDs.

The transparent conductors made of CuNWs become flexible when they are transferred to flexible substrates, such as PET films. The CuNWs/PET films exhibited excellent anti-fatigue performance, and the resistance was almost unchanged after 1000 bending cycles. As a comparison, the resistance of ITO/PET dramatically increased with several bending cycles (Fig. 12d) [158]. The flexible Cu-based transparent conductor was used to fabricate a resistive touch panel, consisting of two layers of Ag coated CuNW transparent networks separated by an insulating spacer. A direct writing on the top surface of the resistive touch panel led to the display of the written letters (Fig. 12e–g) [141].

Solar cells

Solar cells are one type of optoelectronics that require an alternative to the conventional transparent conductor ITO, and Cu-based transparent conductors are very suitable for the ITO replacement (Table S3). The flexible

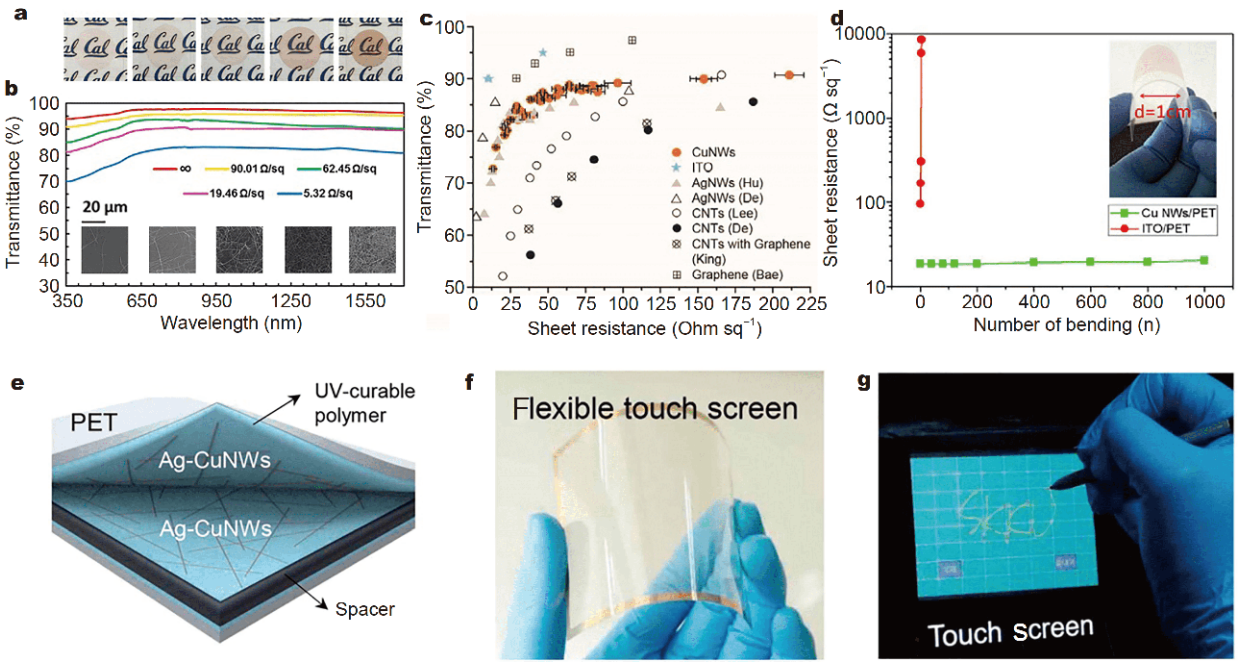

Figure 12 Copper-based soft transparent electrodes. (a) Optical images of ultrathin transparent electrodes with increasing CuNWs loading amounts (from left to right). (b) Wavelength-dependent transmittance, sheet resistance, and corresponding SEM images of transparent conductors. (a, b) Reprinted with permission from Ref. [65]. Copyright 2015, American Chemical Society. (c) Plot of transmittance at a wavelength of 550 nm *versus* sheet resistance for films of CuNWs, AgNWs, ITO, graphene, and CNTs. Reprinted with permission from Ref. [49]. Copyright 2011, Wiley-VCH. (d) Plot of sheet resistance *versus* bending cycles for CuNWs/PET and ITO/PET. The inset is a CuNWs/PET film under bending condition. Reprinted with permission from Ref. [158]. Copyright 2016, Elsevier. (e) Schematic of the device structure, (f) optical image of the flexible touch screen based on Ag coated CuNWs, and (g) the operation of resistive touch screen panel based on Ag coated CuNWs electrodes. Reprinted with permission from Ref. [141]. Copyright 2018, American Chemical Society.

nature of Cu-based transparent conductors additionally makes possible the flexible or stretchable solar cells, which are highly desired in future electronics applications [159,160]. Till now, Cu-based transparent conductors have been successfully used in polymer solar cells [15,161–165], perovskite solar cells [166], and semiconductor-liquid junction solar cells [167].

The high roughness of CuNWs networks has been a major hurdle affecting the performance of solar cells. In order to reduce the roughness of the conductive network, PEDOT:PSS is spin-coated on top of CuNWs, and at the mean time serves as a protection layer to avoid the oxidation of Cu [164]. An alternative way is used by embedding the spray-coated CuNWs on a smooth PEDOT:PSS film [162].

Fig. 13a shows the fabrication procedure for semi-transparent polymer solar cells with CuNWs electrodes for both anodes and cathodes [15]. The flexible CuNWs transparent electrodes were fabricated by a two-step transfer process. CuNWs were first transferred to glass slides at the first step, and they were picked up by polymer layers made of polyacrylates and PI. A subsequent coating of PEDOT:PSS further reduced the roughness of transparent electrodes. *D*-sorbitol was used to modify the surface and electromechanical properties of the electrodes. The polymer solar cells have an inverted structure with layers of polyacrylate/CuNWs/(PEDOT:PSS)/TiO_2/poly(3-hexylthiophene):[6,6]-phenyl-C_{61}-butyric acid 3,4,5-tris(octyloxy)benzyl(P3HT:PC_{61}BM)/PEDOT:PSS/CuNWs/PI/PDMS. The *J*-*V* curves of the PSCs with different concentrations of *D*-sorbitol are presented in Fig. 13b. The solar cells demonstrated average transmittance of 42%, power convention efficiencies (PCE) of 1.97% (1.85%), open circuit voltages (V_{OC}) of 0.62 V (0.62 V), short circuit current densities (J_{SC}) of 7.08 mA cm^{-2} (6.97 mA cm^{-2}), and filling factor (FF) of 0.45 (0.43) when illuminated from the top (bottom) side [15]. The same research group also introduced TiO_2 treatment to improve the conductivity of CuNWs transparent conductors [163]. The flexible polymer solar cells show a PCE of 3.11%, V_{OC} of 0.60 V, J_{SC} of 9.63 mA cm^{-2} and FF of 51%, outperforming the control devices that used ITO-PET electrodes [163]. The PCE of the solar cells using Cu-based transparent conductors remained at 90%

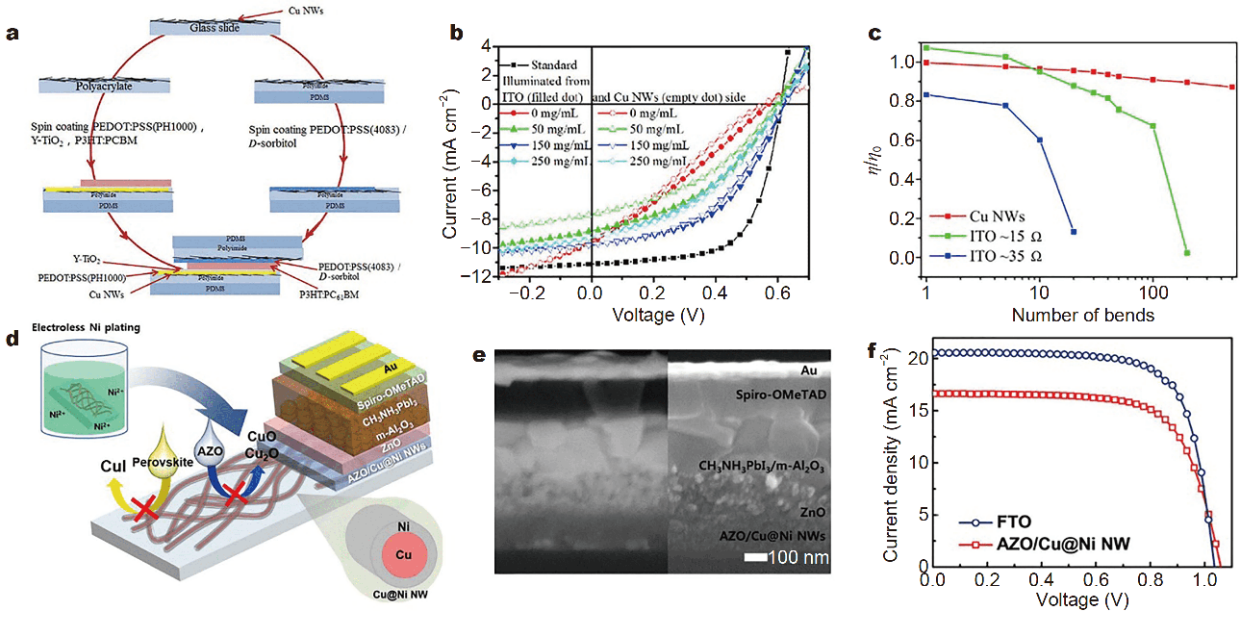

Figure 13 Copper-based soft transparent electrodes for solar cells. (a) Schematic of the preparation procedure of the polymer solar cells with both CuNWs electrodes. (b) *J*-*V* curves of the polymer solar cells with different concentrations of *D*-sorbitol. (a, b) Reprinted with permission from Ref. [15]. Copyright 2018, Springer. (c) The PCE variation of the flexible polymer solar cells based on ITO/PET and CuNWs/polyacrylate electrodes during the bending test. Reprinted with permission from Ref. [163]. Copyright 2018, Springer. (d) Device structure of the perovskite solar cells using the highly stable Cu@NiNWs electrodes. (e) Cross-sectional SEM images of a full device employing AZO/Cu@NiNWs as a bottom electrode. (f) *J*-*V* curve of the best device under standard 1 sun AM 1.5 G illumination. Reprinted with permission from Ref. [166]. Copyright 2018, American Chemical Society.

after 500 bending cycles, while the solar cells with ITO/PET failed after 20 cycles (Fig. 13c).

The direct use of CuNWs in perovskite solar cells is challenging, since Cu is susceptible to reacting with the perovskite phase to form CuI as well as the expected oxidation when in contact with the air [166]. Therefore, Ni coated CuNWs are preferred due to their inertness. Al-doped zinc oxide was coated on the CuNWs for better charge collection and additional protection against iodine ions from the perovskite [166]. The solar cell with the architecture shown in Fig. 13d, e demonstrated a PCE of 12.2%, V_{OC} of 1.06 V, J_{SC} of 16.63 mA cm^{-2} and FF of 69.11% (Fig. 13f) [166]. The solar cells maintained 91% of initial PCE after being stored for 500 h at room temperature [166].

Light-emitting diodes

Cu-based transparent conductors are also capable of replacing ITO in LEDs [16,17,106,141] (Table S4). Lowering the roughness of Cu-based thin film conductor has been one of the research concerns. Similar to the studies in solar cells, PEDOT:PSS has been used to smooth the surface of CuNWs networks [90]. Alternatively, chitosan was used to fill the gaps between CuNWs, resulting in a low roughness composite transparent conductor with improved transmittance [16]. In other cases, the hole injection layers in contact with CuNWs are thicker to eliminate the adverse effect of high roughness of CuNWs surfaces [106]. In order to make a flexible LED, copper-based transparent conductors are basically able to replace the rigid ITO in any organic LEDs architecture.

The structure of the first reported flexible organic LEDs involving Cu-based transparent conductors is shown in Fig. 14a [90]. The LED consisted of CuNWs transferred on a glass-fiber reinforced plastic film, 50 nm thick PEDOT:PSS, 60 nm thick yellow light-emitting polymer, 20 nm thick ZnO layer, and 100 nm thick Al. The fabricated LED had similar luminance-voltage curves to the reference devices fabricated on ITO/glass (Fig. 14b), and exhibited a stable operation in a flexed state (Fig. 14c) [90]. The Cu-based transparent conductors have also been used in green phosphorescent organic LEDs [106]. The device had a structure of CuNWs TCE/HAT-CN (200 nm)/α-NPB (40 nm)/CBP:Ir(ppy)$_3$ (10%, 20 nm)/BCP (10 nm)/Alq$_3$ (40 nm)/LiF (1 nm)/Al (120 nm), in which 1,4,5,8,9,11-hexaazatriphenylene-hexacarbonitrile (HAT-CN) was the hole injection layer, and *N*,*N*′-di(naphthalene-1-yl)-*N*,*N*′-disphenyl-benzidine (α-NPB)

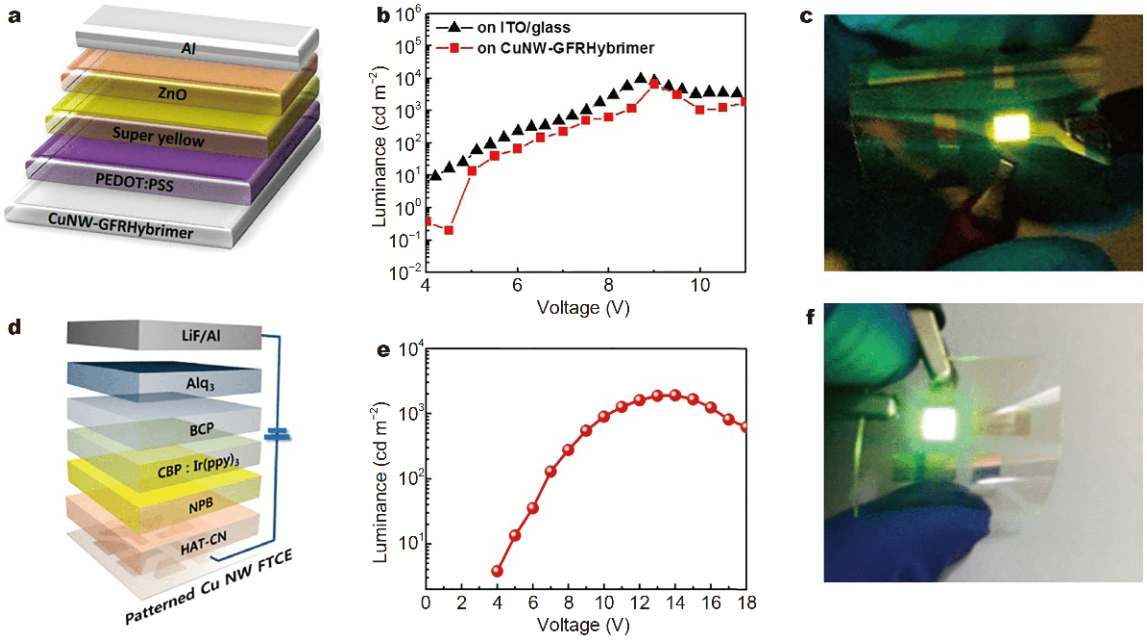

Figure 14 Copper-based soft transparent electrodes for LEDs. (a) Device structure of the flexible organic LED on the Cu-based transparent conductive film. (b) A plot of luminance *vs.* voltage (*L*-*V*) for the flexible organic LED applying the Cu-based transparent electrodes compared with the reference organic LED device on ITO/glass. (c) A photograph of the organic LED device operating at the flexed state. Reprinted with permission from Ref. [90]. Copyright 2014, American Chemical Society. (d) Device structure of a flexible green phosphorescent organic LED constructed on a windmill shaped CuNWs flexible transparent electrode as the anode. (e) Luminance characteristics of the green phosphorescent organic LED device. (f) The photograph of a flexible green phosphorescent organic LED device. Reprinted with permission from Ref. [106]. Copyright 2016, American Chemical Society.

was the hole transport layer. 4,4′-*N*,*N*′-dicarbazolebipheny (CBP) was the host of the emitting layer, Ir(ppy)$_3$ was the common green phosphorescent dopant, bathocuproine (BCP) was the hole blocking layer, and tris(8-hydroxy-quinolinato) aluminum (Alq$_3$) was the electron transport layer (Fig. 14d) [106]. The luminance of the LED increased monotonically with the bias, with a maximum luminance under the drive voltage of 14 V (Fig. 14e) [106]. In addition, the device still showed a uniform and stable light distribution of green emission even in a bending state (Fig. 14f) [106]. The green phosphorescent organic LEDs presented good electrical performance, high luminescent uniformity and excellent mechanical flexibility [106].

Electromechanical sensors

The intricate interplay between the electrical and mechanical properties of copper-based soft conductors makes them natural candidates for electromechanical sensors (Table S5), which have an electrical feedback in response to mechanical changes of the surroundings. The related strain or stress/pressure sensors may serve as a vital component for advanced artificial intelligence devices, and an integral part in the future internet of things network [168]. Sensors are required to have high sensitivity, stability, reliability and robustness, which should be fulfilled by copper-based devices [88,101,169–173].

Gauge factor, defined by the ratio of relative change of resistance to the mechanical strain, is one of the key factors judging the performance of resistive strain sensors. Searching for high gauge factor within a wide range of strain is eagerly investigated, while a concomitant combination of high stretchability and sensitivity is usually difficult [168]. The Cu nanomaterials/elastomer composites usually have a high stretchability; however, the gauge factor is usually not high, making them only suitable for the detection of simple motions [88,171]. In order to improve the sensitivity at high strain, CuNWs and graphite microflakes were combined with additives of HPC into an ink, which could be painted directly and seamlessly on skin to form a sensing device [173]. This strategy made use of the high stretchability of CuNWs embedded in a polymer matrix and high sensitivity of graphite microflakes [173]. With a fractal shaped elastomeric substrates (Fig. 15a), the stretchability was further improved to 600% with a maximum gauge factor of 3000

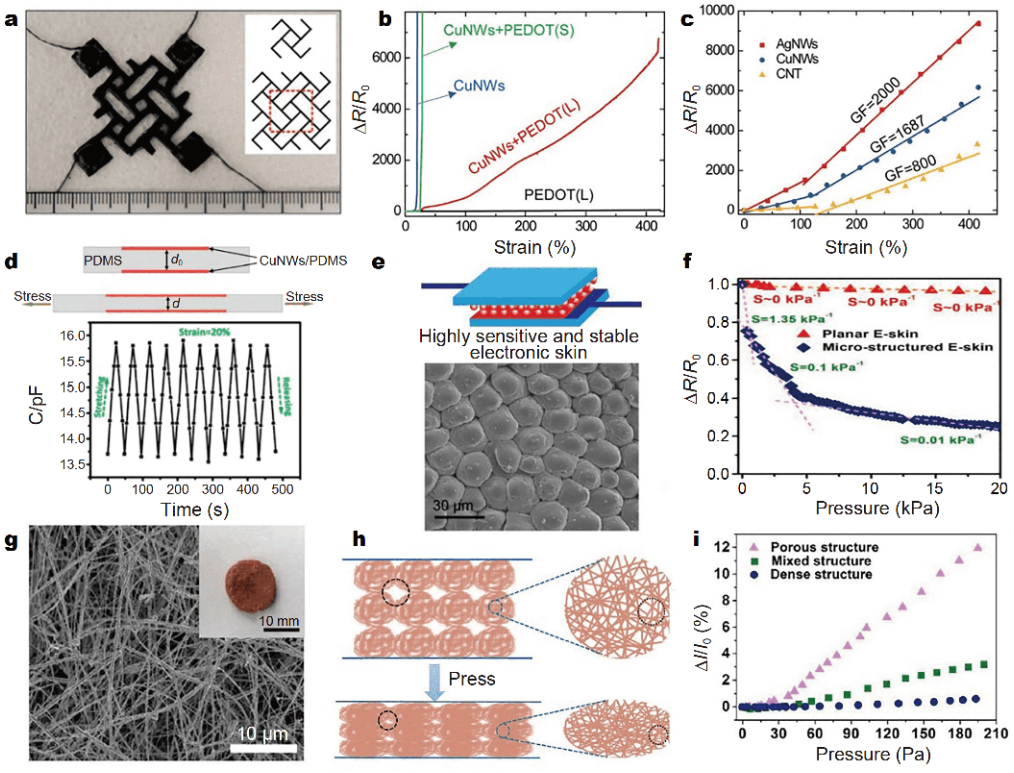

Figure 15 Copper-based electromechanical sensors. (a) The second order fractal zigzag pattern biaxial and torsion graphite microflakes sensors with the first and second order patterns in the inset schematics. Reprinted with permission from Ref. [173]. Copyright 2016, the Royal Society of Chemistry. (b) Relative resistance variations of the copper-based sensors during stretching. (c) Relative resistance changes of the sensors based on AgNWs, CuNWs, or carbon nanotubes from 0% to 420% strain. Reprinted with permission from Ref. [170]. Copyright 2018, Nature Publication Group. (d) Schematic of a capacitive strain sensor with CuNWs/PDMS as the electrodes before and after being stretched, and the plot of change in capacitance *versus* time over ten stretching/releasing cycles under 20% stretching strain with a stretching/releasing speed of 50%/min. Reprinted with permission from Ref. [95]. Copyright 2016, American Chemical Society. (e) Schematic of the fabricated flexible micro-structured electronic skin with similar petal surface structure, and the surface SEM image of the PDMS/Cu-AgNWs composites. (f) Relative resistance change-pressure curve for the electronic skin with petal molded micro-structure and planar surface. Reprinted with permission from Ref. [148]. Copyright 2015, the Royal Society of Chemistry. (g) SEM image of the as-prepared dense CuNWs aerogel and the final product shown in the inset. (h) Illustration of the pore structure of the CuNWs aerogel variation before and after press. (i) Pressure-response curves for porous structure aerogel, mixed structure aerogel and dense structure aerogel, respectively. Reprinted with permission from Ref. [172]. Copyright 2017, American Chemical Society.

[173]. It is worth mentioning that the assembly of CuNWs alone without polymers is brittle, and only allows small strains. By hybridizing CuNWs with the conductive solution of PEDOT:PSS, it was possible to produce a sensor with a high gauge factor at wide ranges for multiscale sensing (Fig. 15b) [170]. Similar concept was applied in Ag NWs and carbon nanotubes sensors, and Cu-based sensors demonstrated a comparable or better performance (Fig. 15c) [170]. As a demonstration, the sensors were able to detect large scale deformations such as skeleton motion, and small-scale deformations such as facial expressions and pulses [170].

Capacitance-type strain sensors have also been made by placing the conductive CuNWs networks on the two sides of the insulating PDMS, forming a parallel plate capacitor. The mechanism of the sensing is based on the capacitance change in response to the PDMS thickness change in correspondence to the strain (Fig. 15d). The gauge factor defined by the capacitance change divided by the applied strain was 0.82, and outperformed other reported results [95]. This sensor had a minimum detectable strain of 1%, and was durable for 1000 cycles of stretching and releasing [95].

In addition to the strain sensors, pressure sensors have also been made from Cu nanomaterials. A highly sensitive and stable flexible electronic skin was fabricated with Ag covered CuNWs coated on PDMS with surface structure replicated from a piece of rose petal (Fig. 15e) [148]. Such a microstructure was used for the purpose of reducing the response time and large hysteresis of elas-

tomers, and improving the pressure sensitivity [174]. The pressure sensor with high sensitivity (1.35 kPa^{-1}, Fig. 15f), very low detection limit (<2 Pa), very low response time and relaxation time (36 and 30 ms) and outstanding working stability (more than 5000 cycles) has extensive applications in voice recognition, wrist pulse monitoring and pressure mapping [148]. Other than thin films, CuNWs based porous 3D structures, such as aerogels (Fig. 15g), have been used for pressure sensors [169,172,175]. The pore structures of the CuNWs aerogel were changed under the pressure, therefore leading to the resistance change of the network (Fig. 15h). The sensitivities (0.02 to 0.7 kPa^{-1}) of this ultralight flexible pressure sensors were negatively correlated to the density of the aerogel sensors (Fig. 15i) [172]. The pressure induced changes in resistance in CuNWs aerogels were quite repeatable for more than 10^4 loading-unloading cycles [175].

Wearable heaters

The low resistance of copper-based soft conductors enables an immediate generation of heat when a suitable bias is applied, therefore they are applied as wearable heaters for thermotherapy or maintaining warmth [88,109,176,177] (Table S6).

In order to make an air-permeable elastic heating patch, stretchable heating fibers were made by incorporating CuNWs into polyester yarns with a protection layer of silicone rubber. These fibers were weaved into the heating fabric, which was integrated into the smart personal heating system controlled by a microcontroller chip (Fig. 16a) [176]. The heating fibers were able to be heated from 20 to 57°C within 20 s at a bias of 3 V. Infrared (IR) thermal image clearly shows a working

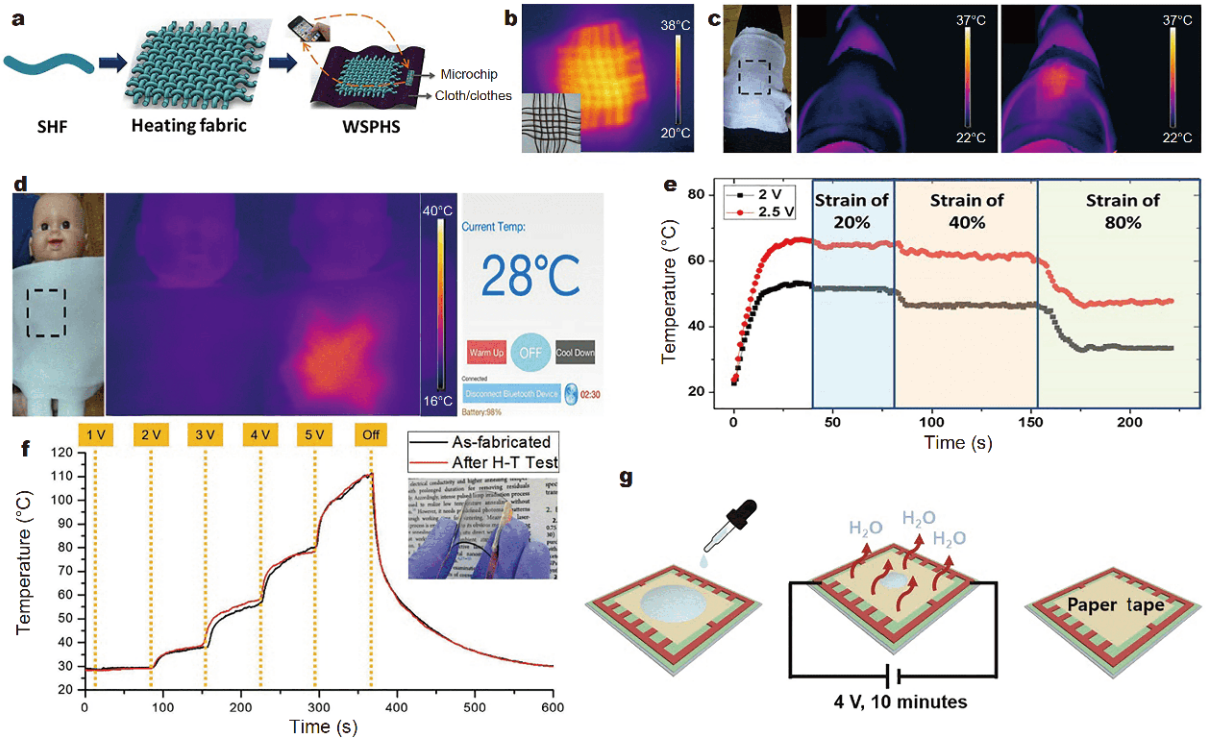

Figure 16 Copper-based wearable heaters. (a) Process schematic of the integration of stretchable heating fiber (SHF) into wearable and smart personal heating system (WSPHS). (b) IR thermal image of heating fabric under direct current (dc) voltage of 1.8 V and photograph of heating fabric. (c, d) Practical wearable applications: (c) photograph of WSPHS application at the knee position (marked by the dotted box) of a human body. IR thermal images before and after switching on the device. (d) Photograph of WSPHS application at the chest position (marked by the dotted box) of an infant model. IR thermal images before and after switching on the device, and the interface on an Android phone reading the body temperature and controlled the heating temperature. (e) Time-dependent temperature curves of SHF being stretched to strains of 20%, 40%, and 80% consecutively under dc voltages of 2 and 2.5 V. (a–e) Reprinted with permission from Ref. [176]. Copyright 2016, American Chemical Society. (f) Transparent and flexible Cu Joule heater demonstration. Transient temperature measurement of the transferred and acid-assisted laser sintering treated Cu electrode under increasing voltage condition from 1 to 5 V. The inset picture represents a digital image of the flexible and transparent heater with the transparency around 85%. (g) A schematic of a flexible heater/drier with wet paper tape. The wet paper loses its water weight after 10 min with 4 V of applied voltage heating condition. Reprinted with permission from Ref. [109]. Copyright, 2017, Wiley-VCH.

wearable heater made of the heating fabric under the low voltage of 1.8 V (Fig. 16b). The heating patch was used for thermotherapy at the knee or chest position of a human body, and the temperature were easily controlled by adjusting the voltage supply (Fig. 16c, d). Under the stretchable conditions, the heating fibers worked well for a strain of 80%, although the temperature was lowered due to the increased resistance during stretching (Fig. 16e) [176]. CuNPs have also been used in the wearable heater applications. A transparent and flexible conductor was made by CuNPs patterning and transfer to a flexible substrate. The temperature of the conductor was easily adjusted by changing the supplied voltages, and functional in a flexed state (Fig. 16f) [109]. The heating effect was shown in a drying experiment, in which a wetted paper lost the water after 10 min of heating under a voltage of 4 V (Fig. 16g).

CONCLUSIONS AND OUTLOOK

Collectively, the developments in the synthesis and assemblies of Cu nanomaterials provide promising engineering possibilities and cost-effective options for flexible or stretchable soft electronics. The 0D, 1D and 2D Cu nanomaterials protected by antioxidation coatings are expected to replace the expensive gold or silver counterparts currently dominating in the field of soft electronics. The meticulous combination of Cu nanomaterials and elastomers or other polymers enables intrinsic or apparent stretchable/flexible conductors. In conjugation with the solution-based assembly approaches, copper nanomaterials allow economic approaches to fabricate Cu-based soft conductive thin films or patterns integratable to a variety of printable or functional electronics, such as smart robotics, electronic skin, optoelectronics, human motion and health monitoring systems, and human-machine interactive systems.

There are still several challenges to overcome for copper nanomaterials to completely replace noble metals in these applications without sacrificing their performance. The antioxidation strategy still needs to be improved by searching for an effective protective coating, which does not greatly degrade the electrical properties, enlarge the dimensions of nanomaterials, or affect the stability of Cu nanomaterials in the inks. With this ideal protection approach, Cu nanomaterials can be as stable as Au or Ag, thereby easing the restrictions for the storage, formulation, and application of Cu-based inks. Surface protection using monolayer organic or inorganic films or alloying with other metals may be the prospective strategy for the effective antioxidation of the copper nanomaterials. In addition, scalable and powerful approaches need to be developed for the synthesis of the Cu nanomaterials with designed shapes or dimensions. Currently, 1D CuNWs are more heavily investigated in comparison to other nanomaterials due to the reliable synthesis and their high aspect ratios. 0D and 2D Cu nanomaterials should deserve more attention, as the Au or Ag counterparts have shown advanced features in stretchable conductors and other applications [178,179]. For this purpose, new and effective synthesis methods for CuNPs or CuNFs are highly desired with more effective control of the nucleation and the growth rate. Furthermore, a fundamental understanding of the multiscale structure and property relationship in Cu-based conductive composites is necessary to delineate the effects of micro morphologies, nanoscale Cu surface/polymer interactions, and the mobility of polymer chains. Finally, effective assembly methods with high resolution patterning capability need to be developed. For example, the direct writing of Cu nanomaterials using ultrasmall nozzles might be a way towards directly printing sub-5 μm or even nanoscale Cu features [116]. With improved synthesis, assembly, and advanced understanding of electrical/structural behavior, we envision that Cu-based conductors should be ubiquitous in various soft electronic devices in the future, and play important roles in a more connected world.

Received 19 May 2019; accepted 27 June 2019; published online 13 August 2019

1 Markvicka EJ, Bartlett MD, Huang X, *et al.* An autonomously electrically self-healing liquid metal-elastomer composite for robust soft-matter robotics and electronics. Nat Mater, 2018, 17: 618–624
2 Park JU, Hardy M, Kang SJ, *et al.* High-resolution electrohydrodynamic jet printing. Nat Mater, 2007, 6: 782–789
3 Guo R, Yao S, Sun X, *et al.* Semi-liquid metal and adhesion-selection enabled rolling and transfer (SMART) printing: a general method towards fast fabrication of flexible electronics. Sci China Mater, 2019, 62: 982–994
4 Rogers JA, Someya T, Huang Y. Materials and mechanics for stretchable electronics. Science, 2010, 327: 1603–1607
5 Choi S, Han SI, Jung D, *et al.* Highly conductive, stretchable and biocompatible Ag-Au core-sheath nanowire composite for wearable and implantable bioelectronics. Nat Nanotech, 2018, 13: 1048–1056
6 Gong S, Schwalb W, Wang Y, *et al.* A wearable and highly sensitive pressure sensor with ultrathin gold nanowires. Nat Commun, 2014, 5: 3132
7 Wang S, Xu J, Wang W, *et al.* Skin electronics from scalable fabrication of an intrinsically stretchable transistor array. Nature, 2018, 555: 83–88
8 Kim D, Kwon J, Jung J, *et al.* A transparent and flexible capacitive-force touch pad from high-aspect-ratio copper nanowires with enhanced oxidation resistance for applications in wearable

electronics. Small Methods, 2018, 2: 1800077
9 Hong I, Lee S, Kim D, *et al.* Study on the oxidation of copper nanowire network electrodes for skin mountable flexible, stretchable and wearable electronics applications. Nanotechnology, 2018, 30: 074001
10 Liu YJ, Cao WT, Ma MG, *et al.* Ultrasensitive wearable soft strain sensors of conductive, self-healing, and elastic hydrogels with synergistic "soft and hard" hybrid networks. ACS Appl Mater Interfaces, 2017, 9: 25559–25570
11 Shi R, Lou Z, Chen S, *et al.* Flexible and transparent capacitive pressure sensor with patterned microstructured composite rubber dielectric for wearable touch keyboard application. Sci China Mater, 2018, 61: 1587–1595
12 Jian M, Wang C, Wang Q, *et al.* Advanced carbon materials for flexible and wearable sensors. Sci China Mater, 2017, 60: 1026–1062
13 Liang J, Tong K, Pei Q. A water-based silver-nanowire screen-print ink for the fabrication of stretchable conductors and wearable thin-film transistors. Adv Mater, 2016, 28: 5986–5996
14 Zhang Y, Su L, Manuzzi D, *et al.* Ultrasensitive and selective non-enzymatic glucose detection using copper nanowires. Biosens Bioelectron, 2012, 31: 426–432
15 Zhai H, Li Y, Chen L, *et al.* Semi-transparent polymer solar cells with all-copper nanowire electrodes. Nano Res, 2018, 11: 1956–1966
16 Lian L, Wang H, Dong D, *et al.* Highly robust and ultrasmooth copper nanowire electrode by one-step coating for organic light-emitting diodes. J Mater Chem C, 2018, 6: 9158–9165
17 Wang Y, Liu P, Wang H, *et al.* Flexible organic light-emitting devices with copper nanowire composite transparent conductive electrode. J Mater Sci, 2019, 54: 2343–2350
18 Ho MD, Ling Y, Yap LW, *et al.* Percolating network of ultrathin gold nanowires and silver nanowires toward "invisible" wearable sensors for detecting emotional expression and apexcardiogram. Adv Funct Mater, 2017, 27: 1700845
19 Chun KY, Oh Y, Rho J, *et al.* Highly conductive, printable and stretchable composite films of carbon nanotubes and silver. Nat Nanotech, 2010, 5: 853–857
20 Cheng Y, Wang R, Chan KH, *et al.* A biomimetic conductive tendril for ultrastretchable and integratable electronics, muscles, and sensors. ACS Nano, 2018, 12: 3898–3907
21 Wu H, Huang YA, Xu F, *et al.* Energy harvesters for wearable and stretchable electronics: from flexibility to stretchability. Adv Mater, 2016, 28: 9881–9919
22 Fu X, Li Z, Xu L, *et al.* Amphiphilic core-sheath structured composite fiber for comprehensively performed supercapacitor. Sci China Mater, 2019, 62: 955–964
23 Guo K, Li Y, Li C, *et al.* Compact self-standing layered film assembled by $V_2O_5{\cdot}nH_2O$/CNTs 2D/1D composites for high volumetric capacitance flexible supercapacitors. Sci China Mater, 2019, 62: 936–946
24 Jia R, Li L, Ai Y, *et al.* Self-healable wire-shaped supercapacitors with two twisted $NiCo_2O_4$ coated polyvinyl alcohol hydrogel fibers. Sci China Mater, 2018, 61: 254–262
25 Liu J, Ye J, Pan F, *et al.* Solid-state yet flexible supercapacitors made by inkjet-printing hybrid ink of carbon quantum dots/graphene oxide platelets on paper. Sci China Mater, 2019, 62: 545–554
26 Zang X, Hou Y, Wang T, *et al.* Temperature-resistant and flexible supercapacitors based on 10-inch wafer-scale nanocarbon films. Sci China Mater, 2019, 62: 947–954
27 Zhou J, Chen N, Ge Y, *et al.* Flexible all-solid-state micro-supercapacitor based on Ni fiber electrode coated with MnO_2 and reduced graphene oxide *via* electrochemical deposition. Sci China Mater, 2018, 61: 243–253
28 Li K, Zhang J. Recent advances in flexible supercapacitors based on carbon nanotubes and graphene. Sci China Mater, 2018, 61: 210–232
29 Choi S, Han SI, Kim D, *et al.* High-performance stretchable conductive nanocomposites: materials, processes, and device applications. Chem Soc Rev, 2019, 48: 1566–1595
30 Kim HW, Kim TY, Park HK, *et al.* Hygroscopic auxetic on-skin sensors for easy-to-handle repeated daily use. ACS Appl Mater Interfaces, 2018, 10: 40141–40148
31 José Andrés L, Fe Menéndez M, Gómez D, *et al.* Rapid synthesis of ultra-long silver nanowires for tailor-made transparent conductive electrodes: proof of concept in organic solar cells. Nanotechnology, 2015, 26: 265201
32 Dou L, Cui F, Yu Y, *et al.* Solution-processed copper/reduced-graphene-oxide core/shell nanowire transparent conductors. ACS Nano, 2016, 10: 2600–2606
33 Zhao J, Wen C, Sun R, *et al.* A sequential process of graphene exfoliation and site-selective copper/graphene metallization enabled by multifunctional 1-pyrenebutyric acid tetrabutylammonium salt. ACS Appl Mater Interfaces, 2019, 11: 6448–6455
34 Zhang B, Li W, Jiu J, *et al.* Large-scale and galvanic replacement free synthesis of Cu@Ag core-shell nanowires for flexible electronics. Inorg Chem, 2019, 58: 3374–3381
35 Yin Z, Chen S, Guan Y, *et al.* Copper nanowire dispersion through an electrostatic dispersion mechanism for high-performance flexible transparent conducting films and optoelectronic devices. ACS Appl Mater Interfaces, 2019, 11: 5264–5275
36 Biçer M, Şişman İ. Controlled synthesis of copper nano/microstructures using ascorbic acid in aqueous CTAB solution. Powder Technol, 2010, 198: 279–284
37 Jin M, He G, Zhang H, *et al.* Shape-controlled synthesis of copper nanocrystals in an aqueous solution with glucose as a reducing agent and hexadecylamine as a capping agent. Angew Chem Int Ed, 2011, 50: 10560–10564
38 Kang B, Han S, Kim J, *et al.* One-step fabrication of copper electrode by laser-induced direct local reduction and agglomeration of copper oxide nanoparticle. J Phys Chem C, 2011, 115: 23664–23670
39 Lee Y, Choi J, Jong Lee K, *et al.* Large-scale synthesis of copper nanoparticles by chemically controlled reduction for applications of inkjet-printed electronics. Nanotechnology, 2008, 19: 415604
40 Park BK, Jeong S, Kim D, *et al.* Synthesis and size control of monodisperse copper nanoparticles by polyol method. J Colloid Interface Sci, 2007, 311: 417–424
41 Ruparelia JP, Chatterjee AK, Duttagupta SP, *et al.* Strain specificity in antimicrobial activity of silver and copper nanoparticles. Acta Biomater, 2008, 4: 707–716
42 Salavati-Niasari M, Davar F, Mir N. Synthesis and characterization of metallic copper nanoparticles *via* thermal decomposition. Polyhedron, 2008, 27: 3514–3518
43 Sim H, Lee J, Yu T, *et al.* Size-tunable and scalable synthesis of uniform copper nanocrystals. RSC Adv, 2015, 5: 2756–2761
44 Suh YD, Kwon J, Lee J, *et al.* Maskless fabrication of highly robust, flexible transparent Cu conductor by random crack network

assisted Cu nanoparticle patterning and laser sintering. Adv Electron Mater, 2016, 2: 1600277
45 Yu T, Koh T, Lim B. Synthesis of copper nanoparticles with controlled sizes by reverse micelle method. J Nanosci Nanotechnol, 2013, 13: 3250–3253
46 Thanh NTK, Maclean N, Mahiddine S. Mechanisms of nucleation and growth of nanoparticles in solution. Chem Rev, 2014, 114: 7610–7630
47 van Embden J, Chesman ASR, Jasieniak JJ. The heat-up synthesis of colloidal nanocrystals. Chem Mater, 2015, 27: 2246–2285
48 Yin Y, Alivisatos AP. Colloidal nanocrystal synthesis and the organic-inorganic interface. Nature, 2005, 437: 664–670
49 Rathmell AR, Wiley BJ. The synthesis and coating of long, thin copper nanowires to make flexible, transparent conducting films on plastic substrates. Adv Mater, 2011, 23: 4798–4803
50 Liu Z, Yang Y, Liang J, *et al.* Synthesis of copper nanowires *via* a complex-surfactant-assisted hydrothermal reduction process. J Phys Chem B, 2003, 107: 12658–12661
51 Chang Y, Lye ML, Zeng HC. Large-scale synthesis of high-quality ultralong copper nanowires. Langmuir, 2005, 21: 3746–3748
52 Rathmell AR, Bergin SM, Hua YL, *et al.* The growth mechanism of copper nanowires and their properties in flexible, transparent conducting films. Adv Mater, 2010, 22: 3558–3563
53 Kim MJ, Flowers PF, Stewart IE, *et al.* Ethylenediamine promotes Cu nanowire growth by inhibiting oxidation of Cu(111). J Am Chem Soc, 2017, 139: 277–284
54 Kim MJ, Alvarez S, Yan T, *et al.* Modulating the growth rate, aspect ratio, and yield of copper nanowires with alkylamines. Chem Mater, 2018, 30: 2809–2818
55 Fu QQ, Li YD, Li HH, *et al. In situ* seed-mediated high-yield synthesis of copper nanowires on large scale. Langmuir, 2019, 35: 4364–4369
56 Zhang D, Wang R, Wen M, *et al.* Synthesis of ultralong copper nanowires for high-performance transparent electrodes. J Am Chem Soc, 2012, 134: 14283–14286
57 Huang X, Chen Y, Chiu CY, *et al.* A versatile strategy to the selective synthesis of Cu nanocrystals and the *in situ* conversion to CuRu nanotubes. Nanoscale, 2013, 5: 6284–6290
58 Shi Y, Li H, Chen L, *et al.* Obtaining ultra-long copper nanowires *via* a hydrothermal process. Sci Technol Adv Mat, 2005, 6: 761–765
59 Huang W, Li J, Zhao S, *et al.* Highly electrically conductive and stretchable copper nanowires-based composite for flexible and printable electronics. Compos Sci Technol, 2017, 146: 169–176
60 Ye E, Zhang SY, Liu S, *et al.* Disproportionation for growing copper nanowires and their controlled self-assembly facilitated by ligand exchange. Chem Eur J, 2011, 17: 3074–3077
61 Mohl M, Pusztai P, Kukovecz A, *et al.* Low-temperature large-scale synthesis and electrical testing of ultralong copper nanowires. Langmuir, 2010, 26: 16496–16502
62 Zhang B, Li W, Yang Y, *et al.* Fully embedded CuNWs/PDMS conductor with high oxidation resistance and high conductivity for stretchable electronics. J Mater Sci, 2019, 54: 6381–6392
63 Kevin M, Lim GYR, Ho GW. Facile control of copper nanowire dimensions *via* the Maillard reaction: using food chemistry for fabricating large-scale transparent flexible conductors. Green Chem, 2015, 17: 1120–1126
64 Guo H, Lin N, Chen Y, *et al.* Copper nanowires as fully transparent conductive electrodes. Sci Rep, 2013, 3: 2323
65 Cui F, Yu Y, Dou L, *et al.* Synthesis of ultrathin copper nanowires using tris(trimethylsilyl)silane for high-performance and low-haze transparent conductors. Nano Lett, 2015, 15: 7610–7615
66 Yang X, Hu X, Wang Q, *et al.* Large-scale stretchable semi-embedded copper nanowire transparent conductive films by an electrospinning template. ACS Appl Mater Interfaces, 2017, 9: 26468–26475
67 An S, Jo HS, Kim DY, *et al.* Self-junctioned copper nanofiber transparent flexible conducting film *via* electrospinning and electroplating. Adv Mater, 2016, 28: 7149–7154
68 Dzenis Y. Spinning continuous fibers for nanotechnology. Science, 2004, 304: 1917–1919
69 Li D, Xia Y. Electrospinning of nanofibers: reinventing the wheel? Adv Mater, 2004, 16: 1151–1170
70 Jiang DH, Tsai PC, Kuo CC, *et al.* Facile preparation of Cu/Ag core/shell electrospun nanofibers as highly stable and flexible transparent conductive electrodes for optoelectronic devices. ACS Appl Mater Interfaces, 2019, 11: 10118–10127
71 Khan MQ, Kharaghani D, Nishat N, *et al.* The fabrications and characterizations of antibacterial PVA/Cu nanofibers composite membranes by synthesis of Cu nanoparticles from solution reduction, nanofibers reduction and immersion methods. Mater Res Express, 2019, 6: 075051
72 Nima M, Shayan A, Sadrnezhaad SK, *et al.* Improving the multi-step fabrication approach of copper nanofiber networks based transparent electrode for achieving superb conductivity and transparency. Mater Res Express, 2019, 6: 095098
73 Wu H, Hu L, Rowell MW, *et al.* Electrospun metal nanofiber webs as high-performance transparent electrode. Nano Lett, 2010, 10: 4242–4248
74 Ahire JJ, Neveling DP, Dicks LMT. Polyacrylonitrile (PAN) nanofibres spun with copper nanoparticles: an anti-*Escherichia coli* membrane for water treatment. Appl Microbiol Biotechnol, 2018, 102: 7171–7181
75 Chinnappan A, Lee JKY, Jayathilaka WADM, *et al.* Fabrication of MWCNT/Cu nanofibers *via* electrospinning method and analysis of their electrical conductivity by four-probe method. Int J Hydrogen Energy, 2018, 43: 721–729
76 Zhong W, Li Y, Zhang Q, *et al.* Junction-free copper wires with submicron linewidth for large-area high-performance transparent electrodes. J Mater Chem C, 2019, 7: 6144–6151
77 Xu S, Sun X, Ye H, *et al.* Selective synthesis of copper nanoplates and nanowires *via* a surfactant-assisted hydrothermal process. Mater Chem Phys, 2010, 120: 1–5
78 Pastoriza-Santos I, Sánchez-Iglesias A, Rodríguez-González B, *et al.* Aerobic synthesis of Cu nanoplates with intense plasmon resonances. Small, 2009, 5: 440–443
79 Wang J, Guo X, He Y, *et al.* The synthesis and tribological characteristics of triangular copper nanoplates as a grease additive. RSC Adv, 2017, 7: 40249–40254
80 Wang S, Oh JY, Xu J, *et al.* Skin-inspired electronics: an emerging paradigm. Acc Chem Res, 2018, 51: 1033–1045
81 Yang J, Choi MK, Kim DH, *et al.* Designed assembly and integration of colloidal nanocrystals for device applications. Adv Mater, 2016, 28: 1176–1207
82 Hu W, Wang R, Lu Y, *et al.* An elastomeric transparent composite electrode based on copper nanowires and polyurethane. J Mater Chem C, 2014, 2: 1298–1305
83 Zhang FT, Xu L, Chen JH, *et al.* Electroless deposition metals on poly(dimethylsiloxane) with strong adhesion as flexible and stretchable conductive materials. ACS Appl Mater Interfaces,

2018, 10: 2075–2082
84 Li S, Chen Y, Huang L, *et al.* Large-scale synthesis of well-dispersed copper nanowires in an electric pressure cooker and their application in transparent and conductive networks. Inorg Chem, 2014, 53: 4440–4444
85 Deshmukh R, Calvo M, Schreck M, *et al.* Synthesis, spray deposition, and hot-press transfer of copper nanowires for flexible transparent electrodes. ACS Appl Mater Interfaces, 2018, 10: 20748–20754
86 Hwang H, Kim A, Zhong Z, *et al.* Reducible-shell-derived pure-copper-nanowire network and its application to transparent conducting electrodes. Adv Funct Mater, 2016, 26: 6545–6554
87 Su D, Jiu J, Suganuma K, *et al.* Stretchable transparent conductors based on copper nanowires and polyurethane. In: 2015 IEEE 15th International Conference on Nanotechnology (IEEE-NANO). Rome: IEEE, 2015. 242–245
88 Ding S, Jiu J, Gao Y, *et al.* One-step fabrication of stretchable copper nanowire conductors by a fast photonic sintering technique and its application in wearable devices. ACS Appl Mater Interfaces, 2016, 8: 6190–6199
89 Ahn Y, Jeong Y, Lee D, *et al.* Copper nanowire-graphene core–shell nanostructure for highly stable transparent conducting electrodes. ACS Nano, 2015, 9: 3125–3133
90 Im HG, Jung SH, Jin J, *et al.* Flexible transparent conducting hybrid film using a surface-embedded copper nanowire network: a highly oxidation-resistant copper nanowire electrode for flexible optoelectronics. ACS Nano, 2014, 8: 10973–10979
91 Kholmanov IN, Domingues SH, Chou H, *et al.* Reduced graphene oxide/copper nanowire hybrid films as high-performance transparent electrodes. ACS Nano, 2013, 7: 1811–1816
92 Hwang C, An J, Choi BD, *et al.* Controlled aqueous synthesis of ultra-long copper nanowires for stretchable transparent conducting electrode. J Mater Chem C, 2016, 4: 1441–1447
93 Ding S, Jiu J, Tian Y, *et al.* Fast fabrication of copper nanowire transparent electrodes by a high intensity pulsed light sintering technique in air. Phys Chem Chem Phys, 2015, 17: 31110–31116
94 Sachse C, Weiß N, Gaponik N, *et al.* ITO-free, small-molecule organic solar cells on spray-coated copper-nanowire-based transparent electrodes. Adv Energy Mater, 2014, 4: 1300737
95 Wang T, Wang R, Cheng Y, *et al.* Quasi *in situ* polymerization to fabricate copper nanowire-based stretchable conductor and its applications. ACS Appl Mater Interfaces, 2016, 8: 9297–9304
96 Naghdi S, Rhee K, Hui D, *et al.* A review of conductive metal nanomaterials as conductive, transparent, and flexible coatings, thin films, and conductive fillers: different deposition methods and applications. Coatings, 2018, 8: 278
97 Yang X, Sun M, Bian Y, *et al.* A room-temperature high-conductivity metal printing paradigm with visible-light projection lithography. Adv Funct Mater, 2019, 29: 1807615
98 Vohra A, Schlingman K, Carmichael RS, *et al.* Membrane-interface-elastomer structures for stretchable electronics. Chem, 2018, 4: 1673–1684
99 Han S, Hong S, Ham J, *et al.* Fast plasmonic laser nanowelding for a Cu-nanowire percolation network for flexible transparent conductors and stretchable electronics. Adv Mater, 2014, 26: 5808–5814
100 Han S, Hong S, Yeo J, *et al.* Nanorecycling: monolithic integration of copper and copper oxide nanowire network electrode through selective reversible photothermochemical reduction. Adv Mater, 2015, 27: 6397–6403
101 Zhang Y, Guo J, Xu D, *et al.* Synthesis of ultralong copper nanowires for high-performance flexible transparent conductive electrodes: the effects of polyhydric alcohols. Langmuir, 2018, 34: 3884–3893
102 Song J, Li J, Xu J, *et al.* Superstable transparent conductive Cu@Cu_4Ni nanowire elastomer composites against oxidation, bending, stretching, and twisting for flexible and stretchable optoelectronics. Nano Lett, 2014, 14: 6298–6305
103 Mayousse C, Celle C, Carella A, *et al.* Synthesis and purification of long copper nanowires. Application to high performance flexible transparent electrodes with and without PEDOT:PSS. Nano Res, 2014, 7: 315–324
104 Won Y, Kim A, Lee D, *et al.* Annealing-free fabrication of highly oxidation-resistive copper nanowire composite conductors for photovoltaics. NPG Asia Mater, 2014, 6: e105
105 Krantz J, Richter M, Spallek S, *et al.* Solution-processed metallic nanowire electrodes as indium tin oxide replacement for thin-film solar cells. Adv Funct Mater, 2011, 21: 4784–4787
106 Zhong Z, Lee H, Kang D, *et al.* Continuous patterning of copper nanowire-based transparent conducting electrodes for use in flexible electronic applications. ACS Nano, 2016, 10: 7847–7854
107 Hu L, Kim HS, Lee JY, *et al.* Scalable coating and properties of transparent, flexible, silver nanowire electrodes. ACS Nano, 2010, 4: 2955–2963
108 Hokita Y, Kanzaki M, Sugiyama T, *et al.* High-concentration synthesis of sub-10-nm copper nanoparticles for application to conductive nanoinks. ACS Appl Mater Interfaces, 2015, 7: 19382–19389
109 Kwon J, Cho H, Suh YD, *et al.* Flexible and transparent Cu electronics by low-temperature acid-assisted laser processing of Cu nanoparticles. Adv Mater Technol, 2017, 2: 1600222
110 Kim Y, Lee B, Yang S, *et al.* Use of copper ink for fabricating conductive electrodes and RFID antenna tags by screen printing. Curr Appl Phys, 2012, 12: 473–478
111 Tam SK, Ng KM. High-concentration copper nanoparticles synthesis process for screen-printing conductive paste on flexible substrate. J Nanopart Res, 2015, 17: 466
112 Rong Y, Ming Y, Ji W, *et al.* Toward industrial-scale production of perovskite solar cells: screen printing, slot-die coating, and emerging techniques. J Phys Chem Lett, 2018, 9: 2707–2713
113 Yu X, Shou W, Mahajan BK, *et al.* Materials, processes, and facile manufacturing for bioresorbable electronics: a review. Adv Mater, 2018, 30: 1707624
114 Derby B. Inkjet printing of functional and structural materials: fluid property requirements, feature stability, and resolution. Annu Rev Mater Res, 2010, 40: 395–414
115 Grouchko M, Kamyshny A, Magdassi S. Formation of air-stable copper-silver core-shell nanoparticles for inkjet printing. J Mater Chem, 2009, 19: 3057–3062
116 Ahn BY, Duoss EB, Motala MJ, *et al.* Omnidirectional printing of flexible, stretchable, and spanning silver microelectrodes. Science, 2009, 323: 1590–1593
117 Onses MS, Song C, Williamson L, *et al.* Hierarchical patterns of three-dimensional block-copolymer films formed by electrohydrodynamic jet printing and self-assembly. Nat Nanotech, 2013, 8: 667–675
118 Knapp CE, Metcalf EA, Mrig S, *et al.* Precursors for atmospheric plasma-enhanced sintering: low-temperature inkjet printing of conductive copper. ChemistryOpen, 2018, 7: 850–857
119 Hon KKB, Li L, Hutchings IM. Direct writing technology—ad-

vances and developments. CIRP Ann, 2008, 57: 601–620
120 Ono T, Kuboki Y, Ajishi Y, *et al.* Application of magnetic printing method to hard-disk media with double recording layers. J Appl Phys, 2003, 93: 7774–7776
121 Lee YI, Choa YH. Adhesion enhancement of ink-jet printed conductive copper patterns on a flexible substrate. J Mater Chem, 2012, 22: 12517–12522
122 Li D, Sutton D, Burgess A, *et al.* Conductive copper and nickel lines *via* reactive inkjet printing. J Mater Chem, 2009, 19: 3719–3724
123 Raut NC, Al-Shamery K. Inkjet printing metals on flexible materials for plastic and paper electronics. J Mater Chem C, 2018, 6: 1618–1641
124 Son YH, Jang JY, Kang MK, *et al.* Application of flash-light sintering method to flexible inkjet printing using anti-oxidant copper nanoparticles. Thin Solid Films, 2018, 656: 61–67
125 Jakus AE, Taylor SL, Geisendorfer NR, *et al.* Metallic architectures from 3D-printed powder-based liquid inks. Adv Funct Mater, 2015, 25: 6985–6995
126 Jason NN, Shen W, Cheng W. Copper nanowires as conductive ink for low-cost draw-on electronics. ACS Appl Mater Interfaces, 2015, 7: 16760–16766
127 Kotikian A, Truby RL, Boley JW, *et al.* 3D printing of liquid crystal elastomeric actuators with spatially programed nematic order. Adv Mater, 2018, 30: 1706164
128 Lin NYC, Homan KA, Robinson SS, *et al.* Renal reabsorption in 3D vascularized proximal tubule models. Proc Natl Acad Sci USA, 2019, 116: 5399–5404
129 Valentine AD, Busbee TA, Boley JW, *et al.* Hybrid 3D printing of soft electronics. Adv Mater, 2017, 29: 1703817
130 Cheng M, Jiang Y, Yao W, *et al.* Elevated-temperature 3D printing of hybrid solid-state electrolyte for Li-ion batteries. Adv Mater, 2018, 30: 1800615
131 Yoo J, Jeong S, Kim S, *et al.* A stretchable nanowire UV-Vis-NIR photodetector with high performance. Adv Mater, 2015, 27: 1712–1717
132 Tubío CR, Azuaje J, Escalante L, *et al.* 3D printing of a heterogeneous copper-based catalyst. J Catal, 2016, 334: 110–115
133 Aziz A, Zhang T, Lin YH, *et al.* 1D copper nanowires for flexible printable electronics and high ampacity wires. Nanoscale, 2017, 9: 13104–13111
134 Yue Y, Liu P, Zhang Z, *et al.* Approaching the theoretical elastic strain limit in copper nanowires. Nano Lett, 2011, 11: 3151–3155
135 Peng C, Zhan Y, Lou J. Size-dependent fracture mode transition in copper nanowires. Small, 2012, 8: 1889–1894
136 Toimil Molares ME, Balogh AG, Cornelius TW, *et al.* Fragmentation of nanowires driven by Rayleigh instability. Appl Phys Lett, 2004, 85: 5337–5339
137 Richter G, Hillerich K, Gianola DS, *et al.* Ultrahigh strength single crystalline nanowhiskers grown by physical vapor deposition. Nano Lett, 2009, 9: 3048–3052
138 Xu L, Yang Y, Hu ZW, *et al.* Comparison study on the stability of copper nanowires and their oxidation kinetics in gas and liquid. ACS Nano, 2016, 10: 3823–3834
139 Wang X, Wang R, Shi L, *et al.* Synthesis of metal/bimetal nanowires and their applications as flexible transparent electrodes. Small, 2015, 11: 4737–4744
140 Ye S, Stewart IE, Chen Z, *et al.* How copper nanowires grow and how to control their properties. Acc Chem Res, 2016, 49: 442–451
141 Kang H, Song SJ, Sul YE, *et al.* Epitaxial-growth-induced junction welding of silver nanowire network electrodes. ACS Nano, 2018, 12: 4894–4902
142 Hong I, Roh Y, Koh JS, *et al.* Semipermanent copper nanowire network with an oxidation-proof encapsulation layer. Adv Mater Technol, 2019, 4: 1800422
143 Zhou KL, Han CB, Li CF, *et al.* Highly stable transparent conductive electrodes based on silver–platinum alloy-walled hollow nanowires for optoelectronic devices. ACS Appl Mater Interfaces, 2018, 10: 36128–36135
144 Wang S, Tian Y, Wang C, *et al.* Communication—Ag NW networks enhanced by Ni electroplating for flexible transparent electrodes. J Electrochem Soc, 2018, 165: D328–D330
145 Wang S, Tian Y, Hang C, *et al.* Cohesively enhanced electrical conductivity and thermal stability of silver nanowire networks by nickel ion bridge joining. Sci Rep, 2018, 8: 5260
146 Niu Z, Cui F, Yu Y, *et al.* Ultrathin epitaxial Cu@Au core-shell nanowires for stable transparent conductors. J Am Chem Soc, 2017, 139: 7348–7354
147 Shang S, Kunwar A, Wang Y, *et al.* Synthesis of Cu@Ag core-shell nanoparticles for characterization of thermal stability and electric resistivity. Appl Phys A, 2018, 124: 492
148 Wei Y, Chen S, Lin Y, *et al.* Cu-Ag core-shell nanowires for electronic skin with a petal molded microstructure. J Mater Chem C, 2015, 3: 9594–9602
149 Lee C, Kim NR, Koo J, *et al.* Cu-Ag core-shell nanoparticles with enhanced oxidation stability for printed electronics. Nanotechnology, 2015, 26: 455601
150 Rathmell AR, Nguyen M, Chi M, *et al.* Synthesis of oxidation-resistant cupronickel nanowires for transparent conducting nanowire networks. Nano Lett, 2012, 12: 3193–3199
151 Koo J, Kwon S, Kim NR, *et al.* Ethylenediamine-enhanced oxidation resistivity of a copper surface during water-based copper nanowire synthesis. J Phys Chem C, 2016, 120: 3334–3340
152 Xu M, Li F, Zhang Z, *et al.* Stretchable and multifunctional strain sensors based on 3D graphene foams for active and adaptive tactile imaging. Sci China Mater, 2019, 62: 555–565
153 Wang S, Tian Y, Wang C, *et al.* Chemical and thermal robust trilayer rGO/Ag NWs/GO composite film for wearable heaters. Compos Sci Technol, 2019, 174: 76–83
154 Catenacci MJ, Reyes C, Cruz MA, *et al.* Stretchable conductive composites from Cu-Ag nanowire felt. ACS Nano, 2018, 12: 3689–3698
155 Won Y, Kim A, Yang W, *et al.* A highly stretchable, helical copper nanowire conductor exhibiting a stretchability of 700%. NPG Asia Mater, 2014, 6: e132
156 Kumar A, Zhou C. The race to replace tin-doped indium oxide: which material will win? ACS Nano, 2010, 4: 11–14
157 Tee BCK, Ouyang J. Soft electronically functional polymeric composite materials for a flexible and stretchable digital future. Adv Mater, 2018, 30: 1802560
158 Wang R, Ruan H. Synthesis of copper nanowires and its application to flexible transparent electrode. J Alloys Compd, 2016, 656: 936–943
159 Lipomi DJ, Tee BCK, Vosgueritchian M, *et al.* Stretchable organic solar cells. Adv Mater, 2011, 23: 1771–1775
160 Kaltenbrunner M, White MS, Głowacki ED, *et al.* Ultrathin and lightweight organic solar cells with high flexibility. Nat Commun, 2012, 3: 770
161 Wang X, Wang R, Zhai H, *et al.* Room-temperature surface modification of Cu nanowires and their applications in trans-

parent electrodes, SERS-based sensors, and organic solar cells. ACS Appl Mater Interfaces, 2016, 8: 28831–28837
162 Chen J, Zhou W, Chen J, *et al.* Solution-processed copper nanowire flexible transparent electrodes with PEDOT:PSS as binder, protector and oxide-layer scavenger for polymer solar cells. Nano Res, 2015, 8: 1017–1025
163 Zhai H, Li Y, Chen L, *et al.* Copper nanowire-TiO_2-polyacrylate composite electrodes with high conductivity and smoothness for flexible polymer solar cells. Nano Res, 2018, 11: 1895–1904
164 Stewart IE, Rathmell AR, Yan L, *et al.* Solution-processed copper-nickel nanowire anodes for organic solar cells. Nanoscale, 2014, 6: 5980–5988
165 Georgiou E, Choulis SA, Hermerschmidt F, *et al.* Printed copper nanoparticle metal grids for cost-effective ITO-free solution processed solar cells. Sol RRL, 2018, 2: 1700192
166 Kim K, Kwon HC, Ma S, *et al.* All-solution-processed thermally and chemically stable copper-nickel core-shell nanowire-based composite window electrodes for perovskite solar cells. ACS Appl Mater Interfaces, 2018, 10: 30337–30347
167 Zhai H, Wang R, Wang W, *et al.* Novel fabrication of copper nanowire/cuprous oxidebased semiconductor-liquid junction solar cells. Nano Res, 2015, 8: 3205–3215
168 Zhao S, Li J, Cao D, *et al.* Recent advancements in flexible and stretchable electrodes for electromechanical sensors: strategies, materials, and features. ACS Appl Mater Interfaces, 2017, 9: 12147–12164
169 Huang J, Wang H, Liang B, *et al.* Oriented freeze-casting fabrication of resilient copper nanowire-based aerogel as robust piezoresistive sensor. Chem Eng J, 2019, 364: 28–36
170 Han S, Liu C, Xu H, *et al.* Multiscale nanowire-microfluidic hybrid strain sensors with high sensitivity and stretchability. npj Flex Electron, 2018, 2: 16
171 Zhu Y, Hu Y, Zhu P, *et al.* Enhanced oxidation resistance and electrical conductivity copper nanowires-graphene hybrid films for flexible strain sensors. New J Chem, 2017, 41: 4950–4958
172 Xu X, Wang R, Nie P, *et al.* Copper nanowire-based aerogel with tunable pore structure and its application as flexible pressure sensor. ACS Appl Mater Interfaces, 2017, 9: 14273–14280
173 Jason NN, Wang SJ, Bhanushali S, *et al.* Skin inspired fractal strain sensors using a copper nanowire and graphite microflake hybrid conductive network. Nanoscale, 2016, 8: 16596–16605
174 Mannsfeld SCB, Tee BCK, Stoltenberg RM, *et al.* Highly sensitive flexible pressure sensors with microstructured rubber dielectric layers. Nat Mater, 2010, 9: 859–864
175 Tang Y, Gong S, Chen Y, *et al.* Manufacturable conducting rubber ambers and stretchable conductors from copper nanowire aerogel monoliths. ACS Nano, 2014, 8: 5707–5714
176 Cheng Y, Zhang H, Wang R, *et al.* Highly stretchable and conductive copper nanowire based fibers with hierarchical structure for wearable heaters. ACS Appl Mater Interfaces, 2016, 8: 32925–32933
177 Hussain AM, Lizardo EB, Torres Sevilla GA, *et al.* Ultrastretchable and flexible copper interconnect-based smart patch for adaptive thermotherapy. Adv Healthc Mater, 2015, 4: 665–673
178 Matsuhisa N, Inoue D, Zalar P, *et al.* Printable elastic conductors by *in situ* formation of silver nanoparticles from silver flakes. Nat Mater, 2017, 16: 834–840
179 Kim Y, Zhu J, Yeom B, *et al.* Stretchable nanoparticle conductors with self-organized conductive pathways. Nature, 2013, 500: 59–63

Acknowledgements This work was supported by the National Natural Science Foundation of China (51873088), Tianjin Municipal Science and Technology Commission (18JCZDJC38400) in China, and "the Fundamental Research Funds for the Central Universities", Nankai University (023/63191303).

Author contributions Zhu J and Feng Y proposed the outline of the manuscript and wrote the paper. Both authors discussed and revised the manuscript.

Conflict of interest The authors declare that they have no conflict of interest.

Supplementary information Supporting data are available in the online version of the paper.

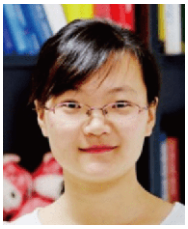

Yang Feng is a postdoctoral fellow in Prof. Jian Zhu's group in the School of Materials Science and Engineering in Nankai University. She received her PhD degree from the University of Chinese Academy of Sciences in 2018. Her research interest is the synthesis of copper nanomaterials, nanoadditive manufacturing for copper-based nanocomposites, and their applications in flexible electronics.

Jian Zhu is a Professor in the School of Materials Science and Engineering in Nankai University. He earned his PhD in chemical engineering from the University of Michigan, Ann Arbor, in 2013, and then started his postdoctoral research in the Department of Materials Science and Engineering at Northwestern University. He has been a faculty member in Nankai University since 2017. His research interest includes nanoelectronic materials, nanoadditive manufacturing, and nanocomposites.

基于铜纳米材料及其组装的柔性电子技术

冯阳[1,2], 朱剑[1,2,3,4*]

摘要 柔性电子在可穿戴和生物植入等应用中发挥着越来越重要的作用. 柔性电子在实现一定电子功能的同时, 具备变形成任意形状的能力. 该领域在过去的十年里进展显著, 在柔性导体、半导体、介电材料的制备中成果颇多. 在这些材料中, 铜基柔性导体由于其价格低廉, 地球储量丰富, 光、电、机械性能优异, 在柔性、可拉伸电极或者电路互连中有着广阔的应用前景. 在这篇综述中, 我们总结了这些材料的最新进展, 详细讨论了铜纳米材料的合成、组装、抗氧化腐蚀策略以及它们在各个领域的应用(如柔性电极、传感器和其他柔性器件). 最后, 我们讨论了铜基柔性导体为应对更广泛的应用场景仍需面临的一系列挑战.

